UNIVERSITY OF SÃO PAULO
DEPARTMENT OF STRUCTURAL ENGINEERING
SÃO CARLOS SCHOOL OF ENGINEERING

ALAN BOURSCHEIDT SEITENFUSS

On the behavior of a linear elastic peridynamic material

Sobre o comportamento de um material peridinâmico elástico linear

São Carlos

2017

ALAN BOURSCHEIDT SEITENFUSS

On the behavior of a linear elastic peridynamic material

Sobre o comportamento de um material peridinâmico elástico linear

Versão corrigida

(Versão original encontra-se na unidade que aloja o Programa de Pós-graduação)

Masters dissertation submitted to the Department of Structural Engineering, São Carlos School of Engineering, University of São Paulo, in partial fulfillment of the requirements for the degree of Master of Science in Civil Engineering (Structures).

Advisor: Prof. Dr. Adair Roberto Aguiar

São Carlos

2017

Seitenfuss, Alan Bourscheidt
S457o On the behavior of a linear elastic peridynamic material / Sobre o comportamento de um material peridinâmico elástico linear / Alan Bourscheidt Seitenfuss; orientador Adair Roberto Aguiar. São Carlos, 2017.

Dissertação (Mestrado) - Programa de Pós-Graduação em Engenharia Civil(Engenharia de Estruturas) e Área de Concentração em Estruturas -- Escola de Engenharia de São Carlos da Universidade de São Paulo, 2017.

1. Elaticidade Linear. 2. Escala de Comprimento. 3. Teoria Não Local. 4. Função Energia Livre. 5. Barra Finita. I. Título.

ACKNOWLEDGEMENTS

I would first like to thank my advisor Professor Adair Roberto Aguiar from the Department of Structural Engineering at University of São Paulo, for guiding and supporting me over the past two years. I would also like to thank Professor Gianni Royer-Carfagni from the Department of Engineering and Architecture at University of Parma in Italy, for the great contribution to this paper. During his visit to São Carlos, the research which resulted in the second part of this dissertation, and another work, has arisen.

My gratitude extends to CNPQ - Conselho Nacional de Desenvolvimento Científico e Tecnológico – who provided financial support to this work, to colleagues and employees from SET/EESC for receptiveness and attention, and to students from other departments of EESC who have contributed, somehow, as well.

I am extremely thankful to the teachers and professors who have contributed to my education during and before my Master's degree.

Finally, I must express my deep gratitude to my parents for providing me an unconditional support and continuous encouragement throughout my years of study. This accomplishment would not have been possible without them. Thank you.

ABSTRACT

SEITENFUSS, A. B. **On the behavior of a linear elastic peridynamic material.** 2017. 69 p. Dissertation (M. Sc. in Civil Engineering (Structures)) – São Carlos School of Engineering , University of São Paulo, São Carlos, 2017.

The peridynamic theory is a generalization of classical continuum mechanics and takes into account the interaction between material points separated by a finite distance within a peridynamic horizon δ. The parameter δ corresponds to a length scale and is treated as a material property related to the microstructure of the body. Since the balance of linear momentum is written in terms of an integral equation that remains valid in the presence of discontinuities, the peridynamic theory is suitable for studying the material behavior in regions with singularities. The first part of this work concerns the evaluation of the properties of a linear elastic peridynamic material in the context of a three-dimensional state-based peridynamic theory, which uses the difference displacement quotient field in the neighborhood of a material point and considers both length and relative angle changes. This material model is based upon a free energy function that contains four material constants, being, therefore, different from other peridynamic models found in the literature, which contain only two material constants.
Using convergence results of the peridynamic theory to the classical linear elasticity theory in the limit of small horizons and a correspondence argument between the free energy function and the strain energy density function from the classical theory, expressions were obtained previously relating three peridynamic constants to the classical elastic constants of an isotropic linear elastic material. To calculate the fourth peridynamic material constant, which couples both bond length and relative angle changes, the correspondence argument is used once again together with the strain field of a linearly elastic beam subjected to pure bending. The expression for the fourth constant is obtained in terms of the Poisson's ratio and the shear elastic modulus of the classical theory. The validity of this expression is confirmed through the consideration of other experiments in mechanics, such as bending of a beam by terminal loads and anti-plane shear of a circular cylinder. In particular, numerical results indicate that the expressions for the constants are independent of the experiment chosen.
The second part of this work concerns an investigation of the behavior of a one-dimensional linearly elastic bar of length L in the context of the peridynamic theory; especially, near the ends of the bar, where it is expected that the behavior of the peridynamic bar may be very different from the behavior of a classical linear elastic bar. The bar is in equilibrium without body force, is fixed at one end, and is subjected to an imposed displacement at the other end. The bar has micromodulus C, which is related to the Young's modulus E in the classical theory through different expressions found in the literature. Depending on the expression for C, the displacement field may be singular near the ends, which is in contrast to the linear behavior of the displacement field observed in classical linear elasticity. In spite of the above, it is also shown that the peridynamic displacement field converges to its classical counterpart as the peridynamic horizon tends to zero.

Keywords: Linear Elasticity. Nonlocal Theory. Free Energy Function. Length Scale. Finite bar. Micromodulus.

RESUMO

SEITENFUSS, A. B. **Sobre o comportamento de um material peridinâmico elástico linear.** 2017. 69 p. Dissertação (Mestrado em Engenharia Civil (Estruturas)) – Escola de Engenharia de São Carlos, Universidade de São Paulo, São Carlos, 2017.

A teoria peridinâmica é uma generalização da teoria clássica da mecânica do contínuo e considera a interação de pontos materiais devido a forças que agem a uma distância finita entre si, além da qual considera-se nula a força de interação. Por ter o balanço de momento linear formulado como uma equação integral que permanece válida na presença de descontinuidades, a teoria peridinâmica é adequada para o estudo do comportamento de materiais em regiões com singularidades. A primeira parte deste trabalho consiste no cálculo das propriedades de um material peridinâmico elástico linear no contexto de uma teoria peridinâmica de estado, linearmente elástica e tridimensional, que utiliza o campo quociente de deslocamento relativo na vizinhança de um ponto material e leva em conta mudanças relativas angulares e de comprimento. Esse modelo utiliza uma função energia livre que apresenta quatro constantes materiais, sendo, portanto, diferente de outros modelos peridinâmicos investigados na literatura, os quais contêm somente duas constantes materiais.
Utilizando resultados de convergência da teoria peridinâmica para a teoria de elasticidade linear clássica no limite de pequenos horizontes e um argumento de correspondência entre as funções energia livre proposta e densidade de energia de deformação da teoria clássica, expressões para três constantes peridinâmicas foram obtidas em função das constantes de um material elástico e isotrópico da teoria clássica. O argumento de correspondêmcia, em conjunto com o campo de deformações de uma viga submetida à flexão pura, é utilizado para calcular a quarta constante peridinâmica do material, que relaciona mudanças angulares relativas e de comprimentos das ligações entre as partículas. Obtem-se uma expressão para a quarta constante em termos do coeficiente de Poisson e do módulo de elasticidade ao cisalhamento da teoria clássica. A validade dessa expressão é confirmada por meio da consideração de outros experimentos da mecânica, tais como flexão de um viga por cargas terminais e cisalhamento anti-plano de um eixo cilíndrico. Em particular, os resultados numéricos indicam que as expressões para as constantes são independentes do experimento escolhido.
A segunda parte deste trabalho consiste em uma investigação do comportamento de uma barra unidimensional linearmente elástica de comprimento L no contexto da teoria peridinâmica; especialmente, próximo às extremidades da barra, onde espera-se que o comportamento da barra peridinâmica possa ser muito diferente do comportamento de uma barra elástica linear clássica. A barra está em equilíbrio e sem força de corpo, fixa em uma extremidade, e sujeita a deslocamento imposto na outra extremidade. A barra possui micromódulo C, o qual está relacionado ao módulo de Young E da teoria clássica por meio de diferentes expressões encontradas na literatura. Dependendo da expressão para C, o campo de deslocamento pode ser singular próximo às extremidades, o que contrasta com o comportamento linear do campo de deslocamento observado na elasticidade linear clássica. Apesar disso, é mostrado também que o campo de deslocamento peridinâmico converge para o campo de deslocamento da teoria clássica quando o horizonte peridinâmico tende a zero.

Palavras-chave: Elaticidade Linear. Teoria Não Local. Função Energia Livre. Escala de Comprimento. Barra Finita. Micromódulo.

LIST OF FIGURES

LIST OF TABLES

CONTENTS

1 INTRODUCTION

1.1 Presentation and motivation

Fracture mechanics aims to determine whether a crack-like defect will lead a solid to catastrophic failure under normal service loading and is a key tool in improving the mechanical performance of materials and components. The importance of the field is clear when considering structures that do not admit failure.

Far from defects, stresses and deformations are smooth and can be studied in the context of the classical theory of elasticity. This theory is local in the sense that a material point interacts only with its immediate neighbors and that stress at a point depends only on its own deformation. At crack tips and interfaces, displacement fields are not smooth and classical elasticity fails to represent the behavior of materials in their neighborhood. Many techniques have been developed to deal with cracks using classical elasticity; however, they usually require initial knowledge of where cracks are located in the material and how they grow. Thus, classical elasticity is not adequate when considering fracture-related problems (GLAWS, 2014).

Peridynamics is a nonlocal theory of continuum mechanics that considers the interaction of material points due to forces acting at a finite distance. The interaction between particles is considered null when this distance exceeds a certain value δ called peridynamic horizon. As the distance increases and becomes infinitely large, the nonlocal theory turns into the continuous version of the molecular dynamics model (OTERKUS, 2010). Consequently, the nonlocal theory of continuous media establishes a connection between molecular dynamics and classical local continuum mechanics (Fig. 1).

The elastic peridynamic theory is a generalization of the classical elasticity theory in the sense that the peridynamic operators converge to the corresponding operators of the classical elasticity on the small horizon limit. The motivation for developing this theory comes from the intention of modeling the behavior of solids in regions with singularities. In contrast with the classical approach, the balance of linear momentum is formulated as an integral equation that remains valid in the presence of discontinuities, such as in the case of Griffith cracks (SILLING et al., 2007).

The damage is incorporated at the level of interaction between two particles and, thus, the location of the crack and the fracture occur as a consequence of the equation of

Figure 1: Relationship among length scales.

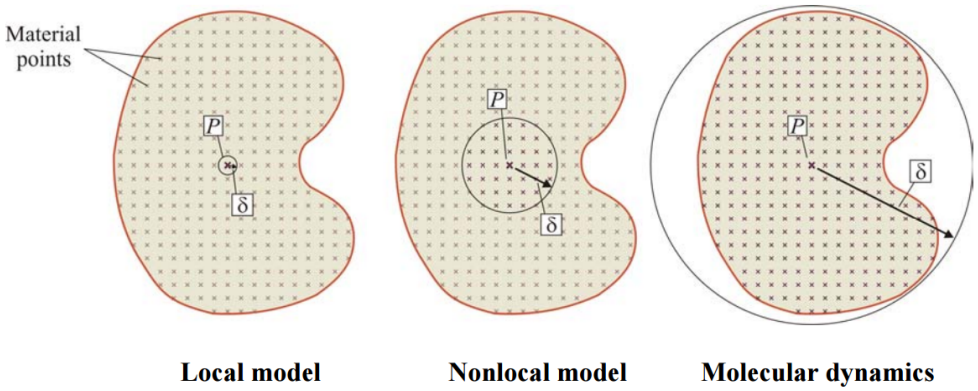

Source: Oterkus (2010).

motion and the constitutive model (SILLING et al., 2007). Cracks start and propagate naturally based on deformation of the material, as opposed to techniques based on classical continuum mechanics, where it is necessary to know the initial position of the crack to predict its propagation.

To achieve the goal of predicting crack formation and propagation, a simple, consistent, and effective material model is needed. The model should be simple enough to be amenable to analysis, verifiable experimentally, and easily implemented in computational codes. It should also be consistent with classical theories away from singular points, such as crack tips and points on interfaces between two different materials, and effective in modeling propagation of cracks and phase interfaces. This work aims at contributing to both the development of the linear peridynamic theory and the modeling of classical problems in mechanics, such as torsion of cylindrical bars, bending of cylindrical beams, and anti-plane shear of hollow cylinders, using a peridynamic model proposed by our group. With a strong theoretical basis, we will extend the results of this investigation to the analysis of fracture mechanics problems, in which formation and propagation of cracks will be the major concern, and phase transitions problems, in which attention will be focused to the formation and propagation of phase interfaces in nonlinear elastic solids with non-convex energy densities.

In this paper, we use a correspondence argument proposed in earlier work together with the non-homogenous deformation of a beam bent by terminal couples to obtain an expression for a fourth peridynamic constant in a material model also proposed earlier in terms of the classical elasticity constants. To verify the validity of the expressions obtained for all peridynamic constants, we consider different experiments in mechanics

and verify that the correspondence argument is nearly satisfied in all cases. In the second part of this work , we investigate linear elastic peridynamic bars of finite length being pulled at the ends. The bars have different expressions for material micromoduli C, which are related to the Young's modulus E in the classical theory. Depending on the micromodulus, numerical results indicate that the displacement field is discontinuous, or, has unbounded derivatives at the ends. Either behavior is in contrast to the homogeneous deformation of the bar predicted by the classical linear theory. Nevertheless, in all cases, the numerical results converge to results obtained from the classical linear theory as a certain scale parameter, called horizon, tends to zero.

1.2 Objectives

The general objective of this work is to contribute, through a theoretical and numerical study, to the development of the peridynamic model proposed by Aguiar e Fosdick (2014).

The specific objectives are listed below.

- To determine the peridynamic constant ($\hat{\alpha}_{13}$) of the model proposed by Aguiar e Fosdick (2014), relating it to the elastic constants from classical theory;

- To verify the validity of the expressions of the peridynamic constants that appear in this author's model by considering classical problems in mechanics.

- To formulate and to solve one-dimensional peridynamic bar problems and investigate nonlocal effects; especially, near the bar ends.

- To analyze the results of the peridynamic bar problem and the effect of the micromodulus choice.

1.3 Structure of the dissertation

In Section 2 we review the literature on peridynamics by discussing some recent developments of the theory, applications of the theory on practical problems, and investigations of one-dimensional peridynamic bar problems. In Chapter 3 we recall the three-dimensional state-based linearly elastic peridynamic theory developed by Aguiar e Fosdick (2014). We start by introducing some kinematical concepts on infinitesimal measures of angular distortion and length changes between material points in Section 3.1. In Section 3.2 we present the force response function state of a simple material and restrict

its form based on the free energy function proposed by Aguiar e Fosdick (2014) which is expressed in terms of the infinitesimal measures of deformation. Expressions for the strain energy function and the linearized force vector state proposed by Silling et al. (2007) are presented in Section 3.3. It then is observed that these expressions correspond to particular cases of the expressions proposed by Aguiar e Fosdick (2014). A correspondence argument is introduced and used in the determination of three peridynamic constants that appear in the expressions of these authors.

In Section 4.1 we present the experiment of a cylindrical linear elastic beam bent by terminal couples and the corresponding displacement field in classical theory. The use of this experiment along with the correspondence argument mentioned above allows to obtain a closed-form expression for a fourth peridynamic constant, that appears in the peridynamic model proposed by Aguiar and Fosdick (2014), in Section 4.2. The determination of this constant is one of the main goals of this work. To obtain this constant, we have used a fixed point at the origin of the coordinate system. We then show that the same expression is found if any other point inside the beam is used. In Section 4.3 we consider the experiment of an elastic beam bent by terminal loads and use it to verify the validity of the closed expressions of the four peridynamic constants that appear in the model proposed by Aguiar and Fosdick (2014). For this, we evaluate numerically the free energy function and the classical strain energy density function for this experiment and use these calculations to verify that the correspondence argument mentioned above is approximately satisfied for given values of mechanical and geometrical properties and at several points inside the beam. A similar verification is conducted in Section 4.4, where we consider the experiment of a cylindrical shaft subjected to anti-plane shear.

The other main goal of this work is to investigate the behavior of the displacement field of a one-dimensional linearly elastic bar of length L near its ends in the context of the peridynamic theory. The one-dimensional peridynamic governing equation is presented in Section 5.1. In Section 5.2 we formulate the problem of an elastic peridynamic bar in equilibrium without body force being subjected to imposed displacements at its ends. The problem is then recast in terms of an inhomogeneous Fredholm equation, which assumes a simplified form in the case of a constant micromodulus. In Section 5.3 we present the numerical scheme used to obtain approximate solutions for different expressions of the micromodulus found in the literature. These solutions are highly nonlinear in a boundary

layer near the ends and may be either discontinuous or singular at these ends. We then concentrate our attention on a particular micromodulus that yields a singular behavior of the solution near the ends. Using this micromodulus, we study both convergence of the proposed numerical scheme and convergence of the nonlocal model to the classical linear elastic model as the horizon δ tends to zero. In Chapter 6 we present some concluding remarks.

2 LITERATURE REVIEW

The solutions of problems in fracture mechanics within the classical continuum theory yield infinite stresses at crack tips, as was shown in Griffith (1921)'s pioneering work. In this context, the appearance and growth of cracks are treated separately by introducing external criteria, such as the critical rate of deformation energy release, which is not part of the governing equations of classical continuum mechanics. In addition, a criterion is also necessary for the determination of the direction of propagation of the cracks. The understanding and prediction of the failure processes of a material are more complex due to the presence of mechanisms associated with grain boundary, microcracks, anisotropy, etc, which interfere with the material response in a certain length scale. Since in the local continuous theory a material point is influenced only by the immediately neighboring points, there is no internal length scale that allows to consider the effect of these damage mechanisms (MADENCI; OTERKUS, 2014).

In order to account for long-range effects, the theory of the nonlocal continuum was introduced (ERINGEN; EDELEN, 1972; KRONER, 1967). In this theory, the stress field at the crack tip is limited (ERINGEN; KIM, 1974), rather than the unlimited stress predicted in the classical theory. In spite of obtaining finite stresses at crack tips, this theory still presents discontinuities in the derivative of the displacement field due to the presence of the cracks. A different nonlocal theory proposed by Kunin (1982) circumvented this difficulty by using displacement fields rather than their derivatives.

2.1 Peridynamic theory

Silling (2000) proposes the peridynamic formulation as a new form of the basic equations of the continuum mechanics intending to model discontinuities formed in the material. To describe the interaction between material points, the author supposes the existence of a force function between two particles that depends only on the relative displacement and the relative positions between the particles. Thus, this model, which is called bond-based model, is restricted to relatively simple interactions between two points.

Silling et al. (2007) develop a generalized form of this model, called the state-based model, which allows the response of a material at a point to depend collectively

on the deformation of all bonds connected to the point. In this work, the authors obtain an energy function for the simple elastic peridynamic material that, as in the classical elasticity theory for isotropic materials, depends only upon two material peridynamic constants. The constitutive laws of this model are significantly more general than the constitutive laws of the binding model. This allows more complex material responses to be modeled numerically at the cost of higher computational cost.

Silling (2010) uses the state-based theory to study the behavior of a peridynamic material by applying a small deformation superposed on a large one and introduced the concept of modulus state. The modulus state expresses the material properties of the linearized response and it is obtained from the second Fréchet derivative of the free energy function for an elastic material. In the case that the deformation of a body is smooth and considering that the behavior of a sequence of peridynamic elastic materials does not change in the limit of vanishing distances between material points, Silling (2010) obtains relations between the modulus state and the fourth-order elasticity tensor in classical continuum theory.

Many works have used successfully peridynamics to predict damage in different problems. Examples include the investigations of Gerstle, Sau e Silling (2005) on plain reinforced concrete structures under quasi-static loading and Askari, Xu e Silling (2006) on a composite laminate under low-velocity impact loading. Warren et al. (2009) demonstrate the capability of a nonordinary state-based model for capturing failure based on either the critical equivalent strain or the averaged value of the volumetric strain. The authors capture the failure behavior of the solid using both isotropic notched and un-notched bar subjected to quasi-static loadings. Oterkus, Barut e Madenci (2010) present an approach based on the merger of classical continuum theory and peridynamic theory to capture failure modes in bolted composite lap joints. The simulations capture the dominant failure modes in the region where the bolt is in contact with the laminate, consistently with common failure modes around the bolt hole observed in previous experimental investigations.

Hu, Ha e Bobaru (2012) use peridynamics to analyse dynamic effects of loading on the damage behavior of unidirectional fiber-reinforced composites. The model captures significant differences in the crack propagation behavior when dynamic loadings of different intensities are applied. Hu et al. (2013) simulate fracture patterns caused by

the impact of a spherical projectile on a thin glass plate with a thin polycarbonate backing plate using a peridynamic simplified model. The main fracture patterns observed experimentally are captured by the peridynamic model for the three different projectile velocities tested

Littlewood, Mish e Pierson (2012) apply peridynamics in combination with modal analysis in the prediction of characteristic frequency shifts that occur during the damage evolution process and demonstrate this application on the benchmark problem of a simply supported beam. Oterkus, Guven e Madenci (2012) consider a reinforced concrete panel subjected to multiple load paths to predict residual strength of impact damaged in building components. To demonstrate the effectiveness of the peridynamic theory for assessment of residual strength of structures, they take a panel with steel reinforcements under impact of an rigid penetrator and another subjected to compression. Zhou, Gu e Wang (2015) and Ha, Lee e Hong (2015) simulate successfully the crack propagation process in rock-like materials subjected to uni-axial tensile and compression loads, respectively. Diyaroglu et al. (2016) demonstrate the applicability of peridynamics to accurately predict nonlinear transient deformation and damage behavior of composites under shock or blast types of loadings due to explosions.

Aguiar e Fosdick (2014) present a three-dimensional state-based linearly elastic peridynamic theory using the relative displacement field between particles. The authors propose a free energy function that depends on deformation measures that are analogous to the measures of strain in classical linear elasticity theory and contains four elastic peridynamic constants. Using vanishing sequences of the horizon δ, the authors find two relations between three peridynamic constants and the two Lamé constants of classical linear elasticity.

In order to obtain a third relation, Aguiar (2016) introduces a correspondence argument between the free energy peridynamic function and a weighted average of the energy density function of the classical theory. This argument provides the two relations mentioned above in the case of homogenous deformations, being, therefore, compatible with the theory presented by Aguiar e Fosdick (2014). Aguiar (2016) uses this argument along with the non-homogenous deformation of a circular shaft under uniform torsion to obtain the third relation. This relation along with those two relations mentioned above allow evaluating three of the four peridynamic constants.

Recall from the exposition in previous sections that a goal of this work is to use the correspondence argument to determine the fourth peridynamic constant and to verify the validity of all formulae found thus far for these constants.

2.2 Peridynamic bar

The effects of long-range forces in the peridynamic theory have motivated the study of one-dimensional bars of infinite length made of linearly elastic peridynamic materials. The corresponding problems are formulated in terms of linear Fredholm integral equations, which are solved by Fourier transform techniques; thus, providing Green's functions for general loading applications. These solutions exhibit features that are not found in their counterparts in the classical linear elasticity theory and are shown to converge to these classical solutions in the limit of short-range forces.

One feature of interest was observed by Silling et al. (2007) in the analysis of a bar with constant micromodulus in $(-\delta, \delta)$, where δ is the horizon, under a single concentrated load. Even though the displacement field obtained from the solution of the corresponding static problem in the classical linear theory is bounded and continuous at all points of the bar, its counterpart in the linear peridynamic theory is unbounded at the point where the force is applied.

Some additional works on one-dimensional bars of infinite length made of linearly elastic peridynamic materials include the investigation of Weckner e Abeyaratne (2005) on the one-dimensional dynamic response of an infinite bar composed of a linear microelastic material. For a Riemann-like problem corresponding to a constant initial displacement field and a piecewise constant initial velocity field the authors find peridynamic solution involving a jump discontinuity for all times after the initial continuous displacement field. Dayal e Bhattacharya (2006) apply the peridynamic formulation of the motion of phase boundaries in one dimension to study the kinetics of phase transformations in solids. They examine nucleation by viewing it as a dynamic instability and propose a nucleation criterion, in which nucleation occurs when the defect size reaches a critical value

Mikata (2012) develops a systematic analytical treatment of peristatic and peridynamic problems for a one-dimensional infinite rod. In order to obtain the exact analytical solutions for the problems the author transforms divergent integrals obtained by Fourier transform into singular solutions plus convergent integrals. Wang, Xu e Wang

(2017a, 2017b) derive the static and dynamic Green's functions for one-, two- and three-dimensional infinite domains considering peridynamics and making use of both Fourier transforms and Laplace transforms. Bobaru et al. (2009) investigate adaptive refinement and convergence in one-dimensional peridynamics. They use adaptive and uniform refinement and different continuous and discontinuous micromoduli for static and dynamic elasticity problems in one dimension. They find that using discontinuous micromodulus functions reduces the quadratic rate of convergence to linear result and that solutions obtained on uniform grids were not sensitive to the micromodulus shape, in the limit of horizon going to zero.

In this work we investigate the behavior of linearly elastic peridynamic bars of finite lengths subjected to displacement conditions at their ends. The bars have distinct micromoduli that can be found in the literature. The main findings of this investigation, which shed new light on the behavior of finite peridynamic bars, consist of a highly nonlinear behavior of the bars near their ends. This is in contrast to what is observed in classical linear elasticity, where the deformation is homogeneous.

3 THEORETICAL BASIS

3.1 Kinematics

The three-dimensional state-based linearly elastic peridynamic theory presented in this chapter was developed by Aguiar and Fosdick (2014) and is also presented in Aguiar (2015). The derivations shown in Section 3.3 after (38) were originally presented in Aguiar (2016).

Let $\mathcal{B} \in \mathbb{E}^3$ be the undistorted reference configuration of an elastic body and let $\mathbf{y} := \boldsymbol{\chi}(\mathbf{x}, t)$ be the position of the particle $\mathbf{x} \in \mathcal{B}$ at time $t \geq 0$. Here, a neighborhood of any point $\mathbf{x}_0$ where we consider the collective deformation of the material is a sphere of radius δ centered at $\mathbf{x}_0$, which we denote by $N_\delta(\mathbf{x}_0) \subset \mathcal{B}$. The vector $\boldsymbol{\xi} := \mathbf{x} - \mathbf{x}_0$ is called a bond from $\mathbf{x}$ to $\mathbf{x}_0$, where $\mathbf{x} \in N_\delta$, as illustrated in Fig. 2. The set $\mathcal{H}_\delta(\mathbf{x}_0)$ is the collection of all bonds to $\mathbf{x}_0$.

Figure 2: Reference and deformed configurations of a body.

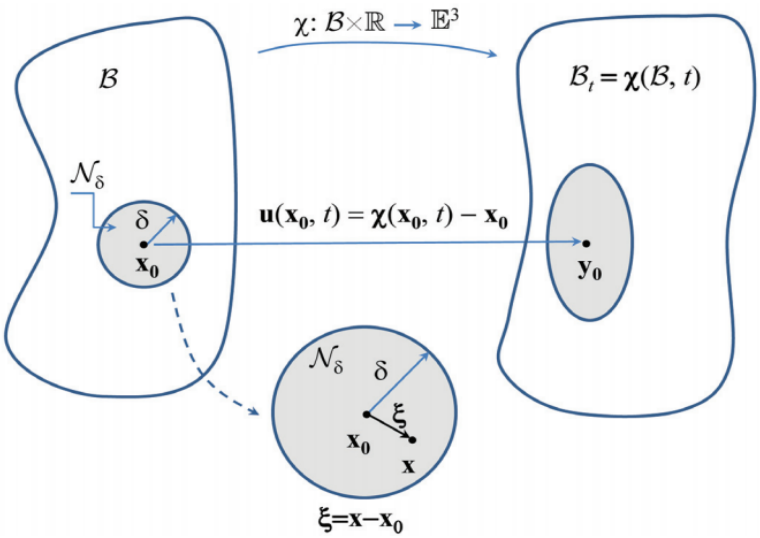

Source: Aguiar e Fosdick (2014).

A peridynamic state at $(\mathbf{x}_0, t)$ of order m is a function $\underline{\mathbf{A}}(\mathbf{x}_0, t)\langle\cdot\rangle : \mathcal{H}_\delta(\mathbf{x}_0) \to \mathcal{L}_m$, where $\mathcal{L}_m$ is the set of all tensors of order m. Thus, the image of a bond $\xi \in \mathcal{H}_\delta(\mathbf{x}_0)$ for the state $\underline{\mathbf{A}}(\mathbf{x}_0, t)\langle\cdot\rangle$ is the tensor of order m, $\underline{\mathbf{A}}(\mathbf{x}_0, t)\langle\boldsymbol{\xi}\rangle$. We denote by $\mathcal{A}_m$ the set of all states at $(\mathbf{x}_0, t)$ of order m. Similarly, we introduce the definition of a double state at $(\mathbf{x}_0, t)$ of order p, $\underline{\underline{\mathbf{D}}}(\mathbf{x}_0, t)\langle\cdot,\cdot\rangle : \mathcal{H}_\delta(\mathbf{x}_0) \times \mathcal{H}_\delta(\mathbf{x}_0) \to \mathcal{L}_p$. The dependency between two states $\underline{\mathbf{A}}(\mathbf{x}_0, t)\langle\cdot\rangle : \mathcal{H}_\delta(\mathbf{x}_0) \to \mathcal{L}_m$ and $\underline{\mathbf{u}}(\mathbf{x}_0, t)\langle\cdot\rangle : \mathcal{H}_\delta(\mathbf{x}_0) \to \mathcal{L}_p$ is denoted by $\underline{\mathbf{A}}(\mathbf{x}_0, t)\langle\boldsymbol{\xi}\rangle = \underline{\widehat{\mathbf{A}}}(\mathbf{x}_0, t)[\underline{\mathbf{u}}]\langle\boldsymbol{\xi}\rangle$. For notational convenience, we shall not exhibit the dependence on the

time variable t and, when the meaning is clear, may also omit the dependence on the particle $\mathbf{x}_0$.

The *difference deformation state* $\underline{\boldsymbol{\chi}} \in \mathcal{A}_1$ at $\mathbf{x}_0 \in \mathcal{B}$ is defined through

$$\underline{\boldsymbol{\chi}}\langle\boldsymbol{\xi}\rangle := (\boldsymbol{\chi}(\mathbf{x}) - \boldsymbol{\chi}(\mathbf{x}_0))\,|_{\mathbf{x}=\mathbf{x}_0+\boldsymbol{\xi}}\,.$$

With $\underline{\mathbf{u}} \in \mathcal{A}_1$ being the *difference displacement state* and $\underline{\mathbf{x}} \in \mathcal{A}_1$ the *reference position vector state* at $\mathbf{x}_0 \in \mathcal{B}$, we may write $\underline{\boldsymbol{\chi}} = \underline{\mathbf{u}} + \underline{\mathbf{x}}$. The *difference deformation* and *displacement quotient states* at $\mathbf{x}_0 \in \mathcal{B}$ are then defined by

$$\underline{\mathbf{f}} := \frac{\underline{\boldsymbol{\chi}}}{|\underline{\mathbf{x}}|} = \underline{\mathbf{h}} + \underline{\mathbf{e}}, \qquad \underline{\mathbf{h}} := \frac{\underline{\mathbf{u}}}{|\underline{\mathbf{x}}|}, \tag{1}$$

respectivelly, where

$$\underline{\mathbf{e}} := \frac{\underline{\mathbf{x}}}{|\underline{\mathbf{x}}|}, \tag{2}$$

and $|\underline{\mathbf{A}}|$ is the *magnitude state* of $\underline{\mathbf{A}}$, defined through

$$|\underline{\mathbf{A}}|\,\langle\boldsymbol{\xi}\rangle := \sqrt{\underline{\mathbf{A}}\langle\boldsymbol{\xi}\rangle \cdot \underline{\mathbf{A}}\langle\boldsymbol{\xi}\rangle}. \tag{3}$$

We select two bonds $\boldsymbol{\xi} = \mathbf{x} - \mathbf{x}_0$ e $\boldsymbol{\eta} = \mathbf{y} - \mathbf{y}_0$ in $\mathcal{H}_\delta$, with $\alpha := \underline{\underline{\alpha}}\langle\boldsymbol{\xi}, \boldsymbol{\eta}\rangle$ being the smallest included angle. We then have that $cos\alpha = \underline{\mathbf{e}}\langle\boldsymbol{\xi}\rangle \cdot \underline{\mathbf{e}}\langle\boldsymbol{\eta}\rangle$. After deformation, the angle will change to $\beta := \underline{\underline{\beta}}\langle\boldsymbol{\xi}, \boldsymbol{\eta}\rangle$, which is determined by

$$cos\beta = \frac{\underline{\boldsymbol{\chi}}\langle\boldsymbol{\xi}\rangle}{|\underline{\boldsymbol{\chi}}\langle\boldsymbol{\xi}\rangle|} \cdot \frac{\underline{\boldsymbol{\chi}}\langle\boldsymbol{\eta}\rangle}{|\underline{\boldsymbol{\chi}}\langle\boldsymbol{\eta}\rangle|} = (\underline{\mathbf{h}}\langle\boldsymbol{\xi}\rangle + \underline{\mathbf{e}}\langle\boldsymbol{\xi}\rangle) \cdot (\underline{\mathbf{h}}\langle\boldsymbol{\eta}\rangle + \underline{\mathbf{e}}\langle\boldsymbol{\eta}\rangle)(\frac{1}{|\underline{\mathbf{f}}\langle\boldsymbol{\xi}\rangle|}\frac{1}{|\underline{\mathbf{f}}\langle\boldsymbol{\eta}\rangle|}). \tag{4}$$

When the deformation of the body is small, we suppose that there is an ϵ, $|\epsilon| < 1$, such that, at $\mathbf{x}_0 \in \mathcal{B}$, $\underline{\mathbf{h}}\langle\boldsymbol{\xi}\rangle \equiv \underline{\mathbf{u}}\langle\boldsymbol{\xi}\rangle/|\boldsymbol{\xi}| = O(\epsilon)$, $|\boldsymbol{\xi}| < \delta$. Using (1) and (3), we get

$$|\underline{\mathbf{f}}\langle\boldsymbol{\xi}\rangle| \equiv \frac{|\underline{\boldsymbol{\chi}}\langle\boldsymbol{\xi}\rangle|}{|\boldsymbol{\xi}|} = 1 + \underline{\mathbf{e}}\langle\boldsymbol{\xi}\rangle \cdot \underline{\mathbf{h}}\langle\boldsymbol{\xi}\rangle + O(\epsilon^2). \tag{5}$$

The strain of a bond $\boldsymbol{\xi}$ at $\mathbf{x}_0$ is defined as the change of length of $\boldsymbol{\xi}$ per unit of length $\boldsymbol{\xi}$ as the result of a deformation, i.e., $\underline{e}\langle\boldsymbol{\xi}\rangle := (|\underline{\boldsymbol{\chi}}| - |\boldsymbol{\xi}|)/|\boldsymbol{\xi}|$. Thus, the infinitesimal normal strain state $\underline{\varepsilon}\langle\cdot\rangle : \mathcal{H}_\delta \to \mathbb{R}$ at $\mathbf{x}_0$ is given by the second term on the right-hand

side of (5), viz.,

$$\underline{\varepsilon}\langle\boldsymbol{\xi}\rangle := \widehat{\underline{\varepsilon}}[\underline{\mathbf{h}}]\langle\boldsymbol{\xi}\rangle \equiv \underline{\mathbf{e}}\langle\boldsymbol{\xi}\rangle \cdot \underline{\mathbf{h}}\langle\boldsymbol{\xi}\rangle. \tag{6}$$

From (6) we see that $\widehat{\underline{\varepsilon}}[\cdot]\langle\boldsymbol{\xi}\rangle : \mathcal{A}_1 \to \mathbb{R}$ is a linear function.

Using (4) and (5), we get

$$cos\beta = cos\alpha + (\underline{\mathbf{e}}\langle\boldsymbol{\xi}\rangle - \underline{\mathbf{e}}\langle\boldsymbol{\eta}\rangle cos\alpha) \cdot \underline{\mathbf{h}}\langle\boldsymbol{\eta}\rangle + (\underline{\mathbf{e}}\langle\boldsymbol{\eta}\rangle - \underline{\mathbf{e}}\langle\boldsymbol{\xi}\rangle cos\alpha) \cdot \underline{\mathbf{h}}\langle\boldsymbol{\xi}\rangle + O(\epsilon^2).$$

Using the trigonometric identities $sin(\alpha-\beta) = sin\alpha\, cos\beta - cos\alpha\, sin\beta$ and $sin\beta = \sqrt{1 - cos^2\beta}$ and linearizing the difference between angles α and β, we get

$$\alpha - \beta = \frac{1}{sin\alpha}[(\underline{\mathbf{e}}\langle\boldsymbol{\xi}\rangle - \underline{\mathbf{e}}\langle\boldsymbol{\eta}\rangle cos\alpha) \cdot \underline{\mathbf{h}}\langle\boldsymbol{\eta}\rangle + (\underline{\mathbf{e}}\langle\boldsymbol{\eta}\rangle - \underline{\mathbf{e}}\langle\boldsymbol{\xi}\rangle cos\alpha) \cdot \underline{\mathbf{h}}\langle\boldsymbol{\xi}\rangle] + O(\epsilon^2).$$

Next, we define the *infinitesimal shear strain state* $\underline{\underline{\gamma}}\langle\cdot,\cdot\rangle : \mathcal{H}_\delta(\mathbf{x}_0) \times \mathcal{H}_\delta(\mathbf{x}_0) \to \mathbb{R}$ through the expression

$$\underline{\underline{\gamma}}\langle\boldsymbol{\xi},\boldsymbol{\eta}\rangle := \widehat{\underline{\underline{\gamma}}}[\mathbf{h}]\langle\boldsymbol{\xi},\boldsymbol{\eta}\rangle \equiv \frac{1}{2}(\underline{\underline{\mathbf{e}}}\langle\boldsymbol{\xi},\boldsymbol{\eta}\rangle \cdot \underline{\mathbf{h}}\langle\boldsymbol{\xi}\rangle + \underline{\underline{\mathbf{e}}}\langle\boldsymbol{\eta},\boldsymbol{\xi}\rangle \cdot \underline{\mathbf{h}}\langle\boldsymbol{\eta}\rangle), \quad |\boldsymbol{\xi}| < \delta,\ |\boldsymbol{\eta}| < \delta, \tag{7}$$

where we have used the notation

$$\underline{\underline{\mathbf{e}}}\langle\boldsymbol{\xi},\boldsymbol{\eta}\rangle := \frac{(\mathbf{1} - \underline{\mathbf{e}}\langle\boldsymbol{\xi}\rangle \otimes \underline{\mathbf{e}}\langle\boldsymbol{\xi}\rangle)\underline{\mathbf{e}}\langle\boldsymbol{\eta}\rangle}{sin\alpha} = \frac{\underline{\mathbf{e}}\langle\boldsymbol{\eta}\rangle - \underline{\mathbf{e}}\langle\boldsymbol{\xi}\rangle cos\alpha}{sin\alpha}, \tag{8}$$

in which $\mathbf{1}$ is the identity tensor in $\mathcal{L}_2$ and α is the smallest included angle between $\boldsymbol{\xi}$ and $\boldsymbol{\eta}$. From (7) and (8) we see that $\widehat{\underline{\underline{\gamma}}}[\cdot]\langle\boldsymbol{\xi},\boldsymbol{\eta}\rangle : \mathcal{A}_1 \to \mathbb{R}$ is also a linear function.

3.2 Simple peridynamic materials

In the state-based theory introduced by Silling et al. (2007), the equation of motion is given by

$$\rho(\mathbf{x}_0)\ddot{\mathbf{u}}(\mathbf{x}_0) = \int_{N_\delta} \{\underline{\mathbf{T}}(\mathbf{x}_0)\langle\mathbf{x} - \mathbf{x}_0\rangle - \underline{\mathbf{T}}(\mathbf{x})\langle\mathbf{x}_0 - \mathbf{x}\rangle\} dv_x + \mathbf{b}(\mathbf{x}_0), \tag{9}$$

where ρ is the mass density in the reference configuration, $\mathbf{u}$ is the displacement field, $\mathbf{b}$ is a prescribed body force density field, both evaluated at $\mathbf{x}_0$, and both $\underline{\mathbf{T}}(\mathbf{x}_0)\langle\cdot\rangle$ and $\underline{\mathbf{T}}(\mathbf{x})\langle\cdot\rangle$ are force vector states evaluated on bonds, respectively, at $\mathbf{x}_0$ and $\mathbf{x}$.

We say that a peridynamic material is simple if, for any $\mathbf{x}_0 \in \mathcal{B}$, there is a force response function state $\underline{\widehat{\mathbf{T}}_{\mathbf{x}_0}}[\cdot]\langle\boldsymbol{\xi}\rangle : \mathcal{A}_1 \to \mathcal{L}_1$, such that

$$\underline{\mathbf{T}} = \underline{\widehat{\mathbf{T}}_{\mathbf{x}_0}}[\underline{\mathbf{f}}].$$

Using both frame indifference and material symmetry conditions, Aguiar e Fosdick (2014) restrict the general form of the force response function. For an isotropic and simple material, the function satisfies the relation

$$\mathbf{Q}^T\underline{\widehat{\mathbf{T}}_{\mathbf{x}_0}}[(\mathbf{Q}\underline{\mathbf{f}}) \circ \underline{\mathbf{q}}^T]\langle\mathbf{Q}\boldsymbol{\xi}\rangle = \underline{\widehat{\mathbf{T}}_{\mathbf{x}_0}}[\underline{\mathbf{f}}]\langle\boldsymbol{\xi}\rangle, \quad \boldsymbol{\xi} \in \mathcal{H}_\delta, \quad \forall \mathbf{Q} \in \mathrm{Orth}^+,$$

where $\underline{\mathbf{q}}^T := \mathbf{Q}^T\underline{\mathbf{x}}$ and Orth^+ is the set of orthogonal positive transformations.

The superposition of a small difference displacement quotient state $\underline{\mathbf{h}}$ onto a difference deformation quotient state $\underline{\check{\mathbf{f}}}$ yields a general expression for the response function of a simple isotropic material in the vicinity of the reference configuration of a peridynamic body, which is given by

$$(\delta_{\underline{\mathbf{f}}}\underline{\widehat{\mathbf{T}}_{\mathbf{x}_0}}[\underline{\mathbf{e}}] \bullet \underline{\mathbf{h}})\langle\boldsymbol{\xi}\rangle = (\mathbf{Q}^T\delta_{\underline{\mathbf{f}}}\underline{\widehat{\mathbf{T}}_{\mathbf{x}_0}}[\underline{\mathbf{e}}] \bullet ((\mathbf{Q}\underline{\mathbf{h}}) \circ \underline{\mathbf{q}}^T))\langle\mathbf{Q}\boldsymbol{\xi}\rangle, \tag{10}$$

where $\underline{\mathbf{e}}$ is given by (2) and $\delta_{\underline{\mathbf{f}}}$ is the Fréchet derivative of a vector state.

The linearized force response function state $\underline{\widehat{\mathbf{L}}_{\mathbf{x}_0}}[\underline{\mathbf{h}}]$ is defined by

$$\underline{\widehat{\mathbf{L}}_{\mathbf{x}_0}}[\underline{\mathbf{h}}] := \underline{\widehat{\mathbf{T}}_{\mathbf{x}_0}}[\underline{\check{\mathbf{f}}}] + \delta_{\underline{\mathbf{f}}}\underline{\widehat{\mathbf{T}}_{\mathbf{x}_0}}[\underline{\check{\mathbf{f}}}] \bullet \underline{\mathbf{h}}. \tag{11}$$

Aguiar e Fosdick (2014) introduce the function $\widehat{\Psi}[\cdot] : \mathcal{A}_1 \to \mathbb{R}$ that represents the free energy at $\mathbf{x}_0$ due to the difference deformation quotient state $\underline{\mathbf{f}}$ at $\mathbf{x}_0$ and show that, for an elastic simple material,

$$\underline{\widehat{\mathbf{T}}_{\mathbf{x}_0}}[\underline{\mathbf{f}}] = \frac{\delta_{\underline{\mathbf{f}}}\underline{\widehat{\Psi}_{\mathbf{x}_0}}[\underline{\mathbf{f}}]}{|\underline{\mathbf{x}}|}. \tag{12}$$

With (12), we can write (11) as

$$\underline{\widehat{\mathbf{L}}_{\mathbf{x}_0}}[\underline{\mathbf{h}}] = \frac{\delta_{\underline{\mathbf{f}}}\underline{\widehat{\Psi}_{\mathbf{x}_0}}[\underline{\check{\mathbf{f}}}]}{|\underline{\mathbf{x}}|} + \frac{(\delta^2_{\underline{\mathbf{f}}}\underline{\widehat{\Psi}_{\mathbf{x}_0}}[\underline{\check{\mathbf{f}}}]) \bullet \underline{\mathbf{h}}}{|\underline{\mathbf{x}}|}. \tag{13}$$

Now, we consider the identity map $\underline{\check{\boldsymbol{\chi}}} = \underline{\mathbf{x}}$, so that $\underline{\check{\mathbf{f}}} = \underline{\mathbf{e}}$ and define the *free energy*

function $\widehat{W}_{\mathbf{x}_0}$ by

$$\widehat{W}_{\mathbf{x}_0}[\underline{\mathbf{h}}] := \frac{1}{2}(\delta^2_{\underline{\mathbf{f}}}\widehat{\Psi}_{\mathbf{x}_0}[\underline{\mathbf{e}}] \bullet \underline{\mathbf{h}}) \bullet \underline{\mathbf{h}}, \tag{14}$$

so that

$$\delta_{\underline{\mathbf{h}}}\widehat{W}_{\mathbf{x}_0}[\underline{\mathbf{h}}] := \delta^2_{\underline{\mathbf{f}}}\widehat{\Psi}_{\mathbf{x}_0}[\underline{\mathbf{e}}] \bullet \underline{\mathbf{h}}. \tag{15}$$

In the case of null residual force state the first term on the right-hand side of (13) is the null tensor, so from (15) and (13) we obtain

$$\underline{\underline{\widehat{\mathbf{L}}}}_{\mathbf{x}_0}[\underline{\mathbf{h}}] = \frac{\delta_{\underline{\mathbf{h}}}\widehat{W}_{\mathbf{x}_0}[\underline{\mathbf{h}}]}{|\underline{\mathbf{x}}|}. \tag{16}$$

Aguiar e Fosdick (2014) propose a free energy function for a simple elastic material that satisfies the invariance condition (10). The function presented below has a quadratic form and uses the infinitesimal strains $\underline{\widehat{\varepsilon}}[\mathbf{h}]$ and $\underline{\underline{\widehat{\gamma}}}[\mathbf{h}]$ defined in (6) and (7), respectively.

$$\begin{aligned}\widehat{W}_{\mathbf{x}_0}[\underline{\mathbf{h}}] = \int_{N_\delta}\int_{N_\delta} \omega(|\boldsymbol{\xi}|,|\boldsymbol{\eta}|)\{&\frac{\alpha_{11}}{2}(\underline{\widehat{\varepsilon}}[\mathbf{h}]\langle\boldsymbol{\xi}\rangle)^2 + \frac{\alpha_{22}}{2}(\underline{\widehat{\varepsilon}}[\mathbf{h}]\langle\boldsymbol{\eta}\rangle)^2 \\ &+ \alpha_{12}\underline{\widehat{\varepsilon}}[\mathbf{h}]\langle\boldsymbol{\xi}\rangle\underline{\widehat{\varepsilon}}[\mathbf{h}]\langle\boldsymbol{\eta}\rangle + \frac{\alpha_{33}}{2}(\underline{\underline{\widehat{\gamma}}}[\mathbf{h}]\langle\boldsymbol{\xi},\boldsymbol{\eta}\rangle)^2 + \alpha_{13}\underline{\underline{\widehat{\gamma}}}[\mathbf{h}]\langle\boldsymbol{\xi},\boldsymbol{\eta}\rangle\underline{\widehat{\varepsilon}}[\mathbf{h}]\langle\boldsymbol{\xi}\rangle \\ &+ \alpha_{23}\underline{\underline{\widehat{\gamma}}}[\mathbf{h}]\langle\boldsymbol{\xi},\boldsymbol{\eta}\rangle\underline{\widehat{\varepsilon}}[\mathbf{h}]\langle\boldsymbol{\eta}\rangle\}dv_\eta dv_\xi,\end{aligned} \tag{17}$$

where $\omega(\cdot,\cdot)$ is a given weighting function and α_{ij}, i, j =1, 2, 3, are elastic peridynamic constants. Assuming that the weighting function $\omega(\cdot,\cdot)$ is symmetric, i.e., $\omega(|\boldsymbol{\xi}|,|\boldsymbol{\eta}|) = \omega(|\boldsymbol{\eta}|,|\boldsymbol{\xi}|)$, we can write (17) as

$$\begin{aligned}\widehat{W}_{\mathbf{x}_0}[\underline{\mathbf{h}}] = \int_{N_\delta}\int_{N_\delta} \omega(|\boldsymbol{\xi}|,|\boldsymbol{\eta}|)\{&\frac{\hat{\alpha}_{11}}{2}(\underline{\widehat{\varepsilon}}[\mathbf{h}]\langle\boldsymbol{\xi}\rangle)^2 + \alpha_{12}\underline{\widehat{\varepsilon}}[\mathbf{h}]\langle\boldsymbol{\xi}\rangle\underline{\widehat{\varepsilon}}[\mathbf{h}]\langle\boldsymbol{\eta}\rangle \\ &+ \frac{\alpha_{33}}{2}(\underline{\underline{\widehat{\gamma}}}[\mathbf{h}]\langle\boldsymbol{\xi},\boldsymbol{\eta}\rangle)^2 + \hat{\alpha}_{13}\underline{\underline{\widehat{\gamma}}}[\mathbf{h}]\langle\boldsymbol{\xi},\boldsymbol{\eta}\rangle\underline{\widehat{\varepsilon}}[\mathbf{h}]\langle\boldsymbol{\xi}\rangle\}dv_\eta dv_\xi,\end{aligned} \tag{18}$$

where we have defined $\hat{\alpha}_{11} := \alpha_{11} + \alpha_{22}$ and $\hat{\alpha}_{13} := \alpha_{13} + \alpha_{23}$.

Replacing (6) and (7) into (18), the free energy function can be rewritten as

$$\begin{aligned}\widehat{W}_{\mathbf{x}_0}[\underline{\mathbf{h}}] = \int_{N_\delta} \underline{\mathbf{h}}\langle\boldsymbol{\xi}\rangle \cdot \int_{N_\delta} \omega(|\boldsymbol{\xi}|,|\boldsymbol{\eta}|)\{&\frac{\hat{\alpha}_{11}}{2}(\underline{\mathbf{e}}\langle\boldsymbol{\xi}\rangle \otimes \underline{\mathbf{e}}\langle\boldsymbol{\xi}\rangle)\underline{\mathbf{h}}\langle\boldsymbol{\xi}\rangle + \alpha_{12}(\underline{\mathbf{e}}\langle\boldsymbol{\xi}\rangle \otimes \underline{\mathbf{e}}\langle\boldsymbol{\eta}\rangle)\underline{\mathbf{h}}\langle\boldsymbol{\eta}\rangle \\ &+ \frac{\alpha_{33}}{4}[(\underline{\underline{\mathbf{e}}}\langle\boldsymbol{\xi},\boldsymbol{\eta}\rangle \otimes \underline{\underline{\mathbf{e}}}\langle\boldsymbol{\xi},\boldsymbol{\eta}\rangle)\underline{\mathbf{h}}\langle\boldsymbol{\xi}\rangle + (\underline{\underline{\mathbf{e}}}\langle\boldsymbol{\eta},\boldsymbol{\xi}\rangle \otimes \underline{\underline{\mathbf{e}}}\langle\boldsymbol{\eta},\boldsymbol{\xi}\rangle)\underline{\mathbf{h}}\langle\boldsymbol{\eta}\rangle] \\ &+ \frac{\hat{\alpha}_{13}}{2}[(\underline{\underline{\mathbf{e}}}\langle\boldsymbol{\xi},\boldsymbol{\eta}\rangle \otimes \underline{\mathbf{e}}\langle\boldsymbol{\xi}\rangle)\underline{\mathbf{h}}\langle\boldsymbol{\xi}\rangle + (\underline{\underline{\mathbf{e}}}\langle\boldsymbol{\xi},\boldsymbol{\eta}\rangle \otimes \underline{\mathbf{e}}\langle\boldsymbol{\eta}\rangle)\underline{\mathbf{h}}\langle\boldsymbol{\eta}\rangle]\}dv_\eta dv_\xi.\end{aligned} \tag{19}$$

Using (19), we get

$$\begin{aligned}\delta_{\underline{\mathbf{h}}}\widehat{W}_{\mathbf{x}_0}[\underline{\mathbf{h}}]\langle\boldsymbol{\xi}\rangle = \int_{N_\delta} \omega(|\boldsymbol{\xi}|,|\boldsymbol{\eta}|)\{&\hat{\alpha}_{11}(\underline{\mathbf{e}}\langle\boldsymbol{\xi}\rangle\otimes\underline{\mathbf{e}}\langle\boldsymbol{\xi}\rangle)\underline{\mathbf{h}}\langle\boldsymbol{\xi}\rangle + \alpha_{12}(\underline{\mathbf{e}}\langle\boldsymbol{\xi}\rangle\otimes\underline{\mathbf{e}}\langle\boldsymbol{\eta}\rangle)\underline{\mathbf{h}}\langle\boldsymbol{\eta}\rangle\\ &+\frac{\alpha_{33}}{2}[(\underline{\underline{\mathbf{e}}}\langle\boldsymbol{\xi},\boldsymbol{\eta}\rangle\otimes\underline{\underline{\mathbf{e}}}\langle\boldsymbol{\xi},\boldsymbol{\eta}\rangle)\underline{\mathbf{h}}\langle\boldsymbol{\xi}\rangle + (\underline{\underline{\mathbf{e}}}\langle\boldsymbol{\eta},\boldsymbol{\xi}\rangle\otimes\underline{\underline{\mathbf{e}}}\langle\boldsymbol{\eta},\boldsymbol{\xi}\rangle)\underline{\mathbf{h}}\langle\boldsymbol{\eta}\rangle]\\ &+\frac{\hat{\alpha}_{13}}{2}[(\underline{\mathbf{e}}\langle\boldsymbol{\xi}\rangle\otimes\underline{\underline{\mathbf{e}}}\langle\boldsymbol{\xi},\boldsymbol{\eta}\rangle + \underline{\underline{\mathbf{e}}}\langle\boldsymbol{\xi},\boldsymbol{\eta}\rangle\otimes\underline{\mathbf{e}}\langle\boldsymbol{\xi}\rangle)\underline{\mathbf{h}}\langle\boldsymbol{\xi}\rangle\\ &+(\underline{\mathbf{e}}\langle\boldsymbol{\eta}\rangle\otimes\underline{\underline{\mathbf{e}}}\langle\boldsymbol{\eta},\boldsymbol{\xi}\rangle + \underline{\underline{\mathbf{e}}}\langle\boldsymbol{\xi},\boldsymbol{\eta}\rangle\otimes\underline{\mathbf{e}}\langle\boldsymbol{\eta}\rangle)\underline{\mathbf{h}}\langle\boldsymbol{\eta}\rangle]\}dv_\eta dv_\xi.\end{aligned}$$

3.3 A linear peridynamic model

By assuming smooth deformation. Lehoucq e Silling (2008) have shown that the peridynamic equation of motion is equivalent to the partial differential equation

$$\rho(\mathbf{x})\ddot{\mathbf{u}}(\mathbf{x}) = \operatorname{div}\mathbf{S}(\mathbf{x}) + \mathbf{b}(\mathbf{x}), \quad \forall\mathbf{x}\in\mathcal{B}, \tag{20}$$

which similar to the equation of motion of the classical theory. In the equation (20), $\mathbf{S}$ is the *peridynamic stress tensor*, given by

$$\mathbf{S}(\mathbf{x}) = \int_{N_1}\int_0^\delta\int_0^\delta (y+z)^2\underline{\mathbf{T}}[\mathbf{x}-z\mathbf{m}]\langle(y+z)\mathbf{m}\rangle\otimes\mathbf{m}\,d\,z\,d\,y\,d\,\Omega_{\mathbf{m}},$$

where $\otimes$ denotes the dyadic product of two vectors, $\underline{\mathbf{T}}$ is the force vector state, N_1 is the unit sphere and $\Omega_{\mathbf{m}}$ is a differential solid angle on N_1 in the direction of any unit vector $\mathbf{m}$.

Let $\widehat{\Psi}_{\mathbf{x}_0}$ be the free energy function at an arbitrary point $\mathbf{x}_0\in\mathcal{B}$. Consider also a family of peridynamic simple elastic materials parameterized by a variable horizon $\delta^s = s\delta$, where δ is held fixed, and given by

$$\widehat{\Psi}^s_{\mathbf{x}_0}[\underline{\mathbf{f}}] := \widehat{\Psi}_{\mathbf{x}_0}[\underline{\mathbf{E}}^s\underline{\mathbf{f}}]. \tag{21}$$

In (21), $\underline{\mathbf{E}}^s$ is an *enlarged difference deformation quotient state* defined by

$$\underline{\mathbf{E}}^s[\underline{\mathbf{f}}]\langle\boldsymbol{\xi}\rangle = \underline{\mathbf{f}}\langle s\boldsymbol{\xi}\rangle, \quad \forall\boldsymbol{\xi}\in\mathcal{H}_\delta,\ \forall\underline{\mathbf{f}}\in\mathcal{A}_1.$$

The peridynamic stress tensor associated with $\widehat{\Psi}^s_{\mathbf{x}_0}$ is given by

$$\mathbf{S}^s(\mathbf{x}_0) = \int_{N_1}\int_0^\delta\int_0^\delta (y+z)^2 \underline{\mathbf{T}_{\mathbf{x}_0 - sz\mathbf{m}}}[\underline{\mathbf{E}}^s[\underline{\mathbf{f}}(\mathbf{x}_0 - sz\mathbf{m})]]\langle (y+z)\mathbf{m}\rangle \otimes \mathbf{m}\, d\, z\, d\, y\, d\, \Omega_{\mathbf{m}}.$$

Assuming that the motion $\boldsymbol{\chi}$ is twice continuously differentiable and that $\underline{\mathbf{T}_{\mathbf{x}_0}}$ is continuously differentiable with respect to $\underline{\boldsymbol{\chi}}$ and to the position $\mathbf{x}$, Silling e Lehoucq (2008) have shown that

$$\lim_{s\to 0} \mathbf{S}^s = \mathbf{P} \quad \text{em } \mathcal{B},$$

where $\mathbf{P}$ is the Piola–Kirchhoff stress field of the classical theory, which is related to the response function $\underline{\mathbf{T}_{\mathbf{x}_0}}$ of a linear peridynamic material by

$$\mathbf{P}(\mathbf{x}_0) = \int_{N_\delta} \underline{\mathbf{T}_{\mathbf{x}_0}}[\mathbf{F}(\mathbf{x}_0)\underline{\mathbf{e}}]\langle\boldsymbol{\xi}\rangle \otimes \boldsymbol{\xi} dv_\xi, \tag{22}$$

and $\mathbf{F}(\mathbf{x}_0)$ is the deformation gradient tensor at $\mathbf{x}_0$ given by

$$\mathbf{F}(\mathbf{x}) = \frac{\partial \boldsymbol{\chi}(\mathbf{x})}{\partial \mathbf{x}} = \mathbf{1} + \mathbf{H}(\mathbf{x}), \quad \mathbf{H}(\mathbf{x}) := \frac{\partial \mathbf{u}(\mathbf{x})}{\partial \mathbf{x}}.$$

Assuming that the displacement gradient $\mathbf{H}_0 := \mathbf{H}(\mathbf{x}_0)$ is small, the expression (22) can be approximated by

$$\mathbf{P}_L(\mathbf{x}_0) = \int_{N_\delta} \delta_{\underline{\mathbf{h}}}\widehat{W}_{\mathbf{x}_0}[\mathbf{H}_0\underline{\mathbf{e}}]\langle\boldsymbol{\xi}\rangle \otimes \underline{\mathbf{e}}\langle\boldsymbol{\xi}\rangle dv_\xi. \tag{23}$$

Taking the inner product between $\mathbf{H}_0$ and $\mathbf{P}_L(\mathbf{x}_0)$ in (23), we obtain

$$\mathbf{H}_0 \cdot \mathbf{P}_L(\mathbf{x}_0) = \int_{N_\delta} tr\left[\delta_{\underline{\mathbf{h}}}\widehat{W}_{\mathbf{x}_0}[\mathbf{H}_0\underline{\mathbf{e}}]\langle\boldsymbol{\xi}\rangle \otimes (\mathbf{H}_0\underline{\mathbf{e}}\langle\boldsymbol{\xi}\rangle)\right] dv_\xi = (\mathbf{H}_0\underline{\mathbf{e}}) \bullet \delta_{\underline{\mathbf{h}}}\widehat{W}_{\mathbf{x}_0}[\mathbf{H}_0\underline{\mathbf{e}}].$$

Using (14) and (15) in the above expression, we get

$$\frac{1}{2}\mathbf{H}_0 \cdot \mathbf{P}_L(\mathbf{x}_0) = \widehat{W}_{\mathbf{x}_0}[\mathbf{H}_0\underline{\mathbf{e}}]. \tag{24}$$

It then follows from the above result that, in the limit of small horizon, both the classical continuum theory and the peridynamic theory yield the same energy at a point $\mathbf{x}_0$ in the vicinity of the reference configuration.

The Generalized Hooke's Law in classical linear elasticity relates the tensor $\mathbf{P}_L(\mathbf{x}_0)$

to the infinitesimal displacement gradient tensor $\mathbf{H}_0$ through $\mathbf{P}_L(\mathbf{x}_0) = \mathbb{C}_{\mathbf{x}_0}\mathbf{H}_0$, where $\mathbb{C}_{\mathbf{x}_0}$ is the elasticity tensor at $\mathbf{x}_0$. Substituting this relation into (24), we get

$$\frac{1}{2}\mathbf{H}_0 \cdot (\mathbb{C}_{\mathbf{x}_0}\mathbf{H}_0) = \widehat{W}_{\mathbf{x}_0}[\mathbf{H}_0\underline{\mathbf{e}}]. \tag{25}$$

For the linearized simple elastic material given by the free energy function (19), we have that

$$\begin{aligned}\frac{1}{2}\mathbf{H}_0 \cdot (\mathbb{C}_{\mathbf{x}_0}\mathbf{H}_0) =& \frac{1}{2}\mathbf{H}_0 \cdot \{\int_{N_\delta}\int_{N_\delta} \omega(|\boldsymbol{\xi}|,|\boldsymbol{\eta}|)[\hat{\alpha}_{11}\ \underline{\mathbf{e}}\langle\boldsymbol{\xi}\rangle \otimes \underline{\mathbf{e}}\langle\boldsymbol{\xi}\rangle \otimes \underline{\mathbf{e}}\langle\boldsymbol{\xi}\rangle \otimes \underline{\mathbf{e}}\langle\boldsymbol{\xi}\rangle \\ &+ 2\alpha_{12}\ \underline{\mathbf{e}}\langle\boldsymbol{\xi}\rangle \otimes \underline{\mathbf{e}}\langle\boldsymbol{\xi}\rangle \otimes \underline{\mathbf{e}}\langle\boldsymbol{\eta}\rangle \otimes \underline{\mathbf{e}}\langle\boldsymbol{\eta}\rangle \\ &+ \frac{\alpha_{33}}{2}\underline{\underline{\mathbf{e}}}\langle\boldsymbol{\xi},\boldsymbol{\eta}\rangle \otimes \underline{\mathbf{e}}\langle\boldsymbol{\xi}\rangle \otimes (\underline{\underline{\mathbf{e}}}\langle\boldsymbol{\xi},\boldsymbol{\eta}\rangle \otimes \underline{\mathbf{e}}\langle\boldsymbol{\xi}\rangle + \underline{\underline{\mathbf{e}}}\langle\boldsymbol{\eta},\boldsymbol{\xi}\rangle \otimes \underline{\mathbf{e}}\langle\boldsymbol{\eta}\rangle) \\ &+ \hat{\alpha}_{13}(\underline{\underline{\mathbf{e}}}\langle\boldsymbol{\xi},\boldsymbol{\eta}\rangle \otimes \underline{\mathbf{e}}\langle\boldsymbol{\xi}\rangle + \underline{\underline{\mathbf{e}}}\langle\boldsymbol{\eta},\boldsymbol{\xi}\rangle \otimes \underline{\mathbf{e}}\langle\boldsymbol{\eta}\rangle) \otimes \underline{\mathbf{e}}\langle\boldsymbol{\xi}\rangle \otimes \underline{\mathbf{e}}\langle\boldsymbol{\xi}\rangle]dv_\eta dv_\xi \mathbf{H}_0\}.\end{aligned} \tag{26}$$

Aguiar e Fosdick (2014) show that all the integral terms that multiply $\hat{\alpha}_{13}$ in the expression (26) vanish. We then conclude that the terms multiplied by $\hat{\alpha}_{13}$ do not contribute to the free energy $\widehat{W}_{\mathbf{x}_0}[\mathbf{H}_0\underline{\mathbf{e}}]$ of a peridynamic body at $\mathbf{x}_0$ in the limit of vanishing horizon.

Being ξ_i, η_i the components of $\underline{\mathbf{x}}\langle\boldsymbol{\xi}\rangle \equiv \boldsymbol{\xi}$ and $\underline{\mathbf{x}}\langle\boldsymbol{\eta}\rangle \equiv \boldsymbol{\eta}$, respectively, and $\{\mathbf{e}_1, \mathbf{e}_2, \mathbf{e}_3\}$ a fixed basis, it follows from (2) that

$$\underline{\mathbf{e}}\langle\boldsymbol{\xi}\rangle := \frac{\xi_i}{|\boldsymbol{\xi}|}\mathbf{e}_i, \quad \underline{\mathbf{e}}\langle\boldsymbol{\eta}\rangle := \frac{\eta_i}{|\boldsymbol{\eta}|}\mathbf{e}_i. \tag{27}$$

Replacing (27) into (8) yields

$$\underline{\underline{\mathbf{e}}}\langle\boldsymbol{\xi},\boldsymbol{\eta}\rangle := \frac{1}{sin\alpha}\left(\frac{\eta_i}{|\boldsymbol{\eta}|} - cos\alpha\frac{\xi_i}{|\boldsymbol{\xi}|}\right)\mathbf{e}_i, \qquad \underline{\underline{\mathbf{e}}}\langle\boldsymbol{\eta},\boldsymbol{\xi}\rangle := \frac{1}{sin\alpha}\left(\frac{\xi_i}{|\boldsymbol{\xi}|} - cos\alpha\frac{\eta_i}{|\boldsymbol{\eta}|}\right)\mathbf{e}_i. \tag{28}$$

With C_{ijkl}, i,j,k,l=1,2,3, being the classical elastic constants and H_{ij} the components of $\mathbf{H}_0$, we write

$$\frac{1}{2}\mathbf{H}_0 \cdot (\mathbb{C}_{\mathbf{x}_0}\mathbf{H}_0) = \frac{1}{2}H_{ij}C_{ijkl}H_{kl}. \tag{29}$$

Substituting (27), (28), and (29) into the expression (26), we get

$$C_{ijkl} = \hat{\alpha}_{11}C^{11}_{ijkl} + \frac{\alpha_{33}}{2}C^{33}_{ijkl} + 2\alpha_{12}C^{12}_{ijkl}, \tag{30}$$

where

$$
\begin{aligned}
C_{ijkl}^{11} &\equiv \int_{N_\delta}\int_{N_\delta} \omega(|\boldsymbol{\xi}|,|\boldsymbol{\eta}|)dv_\eta \frac{\xi_i\xi_j\xi_k\xi_l}{|\boldsymbol{\xi}|^4}dv_\xi,\\
C_{ijkl}^{33} &\equiv \int_{N_\delta}\int_{N_\delta} \frac{\omega(|\boldsymbol{\xi}|,|\boldsymbol{\eta}|)}{sin^2\alpha}\left(\frac{\eta_i}{|\boldsymbol{\eta}|}-cos\alpha\frac{\xi_i}{|\boldsymbol{\xi}|}\right)\frac{\xi_j}{|\boldsymbol{\xi}|}\\
&\quad\left[\left(\frac{\eta_k}{|\boldsymbol{\eta}|}-cos\alpha\frac{\xi_k}{|\boldsymbol{\xi}|}\right)\frac{\xi_l}{|\boldsymbol{\xi}|}+\left(\frac{\xi_k}{|\boldsymbol{\xi}|}-cos\alpha\frac{\eta_k}{|\boldsymbol{\eta}|}\right)\frac{\eta_l}{|\boldsymbol{\eta}|}\right]dv_\eta dv_\xi,\\
C_{ijkl}^{12} &\equiv \int_{N_\delta}\int_{N_\delta} \omega(|\boldsymbol{\xi}|,|\boldsymbol{\eta}|)\frac{\xi_i\xi_j\xi_k\xi_l}{(|\boldsymbol{\xi}||\boldsymbol{\eta}|)^2}dv_\eta dv_\xi.
\end{aligned}
\tag{31}
$$

The Cartesian coordinates ξ_i, η_i are given in terms of the spherical coordinates $(\check{\rho},\check{\theta},\check{\phi}),(\widehat{\rho},\widehat{\theta},\widehat{\phi})$ through

$$
\begin{aligned}
(\xi_1,\xi_2,\xi_3) &= \check{\rho}(cos\check{\theta}\ sin\check{\phi}, sin\check{\theta}\ sin\check{\phi}, cos\check{\phi}),\\
(\eta_1,\eta_2,\eta_3) &= \widehat{\rho}(cos\widehat{\theta}\ sin\widehat{\phi}, sin\widehat{\theta}\ sin\widehat{\phi}, cos\widehat{\phi}).
\end{aligned}
\tag{32}
$$

Substituting (32) into (31) and taking the limits of integration on N_δ as

$$
\rho\in(0,\delta),\ \phi\in(0,\pi) \text{ and } \theta\in(0,2\pi),
\tag{33}
$$

we have the values presented in Tab. 1, in which $\omega_\delta \equiv \pi^2\int_0^\delta\int_0^\delta \omega(\check{\rho},\widehat{\rho})\check{\rho}^2\widehat{\rho}^2 d\widehat{\rho}d\check{\rho}$.

Table 1: Peridynamic coefficients defined in (31).

(i,j,k,l)	$C_{ijkl}^{11}/\omega_\delta$	$C_{ijkl}^{33}/\omega_\delta$	$C_{ijkl}^{12}/\omega_\delta$
(1, 1, 1, 1)	16/5	1.4221≈64/45	16/9
(2, 2, 2, 2)	16/5	1.4221≈64/45	16/9
(3, 3, 3, 3)	16/5	1.4221≈64/45	16/9
(1, 1, 2, 2)	16/5	-0.7111≈-32/45	16/9
(1, 1, 3, 3)	16/5	-0.7111≈-32/45	16/9
(2, 2, 3, 3)	16/5	-0.7111≈-32/45	16/9
(2, 3, 2, 3)	16/5	1.0667≈16/15	0
(1, 3, 1, 3)	16/5	1.0667≈16/15	0
(1, 2, 1, 2)	16/5	1.0667≈16/15	0

The matrices with components C_{ijkl}^{11} e C_{ijkl}^{12} have minor and major symmetries. The symmetry for the coeficients C_{ijkl}^{33} is given by $C_{ijkl}^{33}=C_{jikl}^{33}=C_{ijlk}^{33}=C_{klij}^{33}$. The coefficients

not shown in the table and that do not satisfy the cited simmetries are zero.

Substitution of the values of Tab. 1 into (30) yields a system of equations for the calculations of the constants $\hat{\alpha}_{11}$, α_{12} e α_{33} in terms of the elastic constants C_{ijkl}. This system has no solution unless the following relations are satisfied.

$$\begin{aligned}
&C_{ii23} = C_{ii13} = C_{ii12} = 0,\\
&C_{2313} = C_{1312} = C_{2312} = 0,\\
&C_{2222} = C_{1111} = C_{3333},\\
&C_{1133} = C_{2233} = C_{1122},\\
&C_{2323} = C_{1313} = C_{1212} = (C_{1111} - C_{1122})/2.
\end{aligned} \tag{34}$$

Clearly the values of Tab. 1 substituted in (30) yield elastic constants that satisfy the relations in (34). Also, these relations imply that the classical elastic material must be istropic. Using (30), (34) and Tab. 1, we get the relations

$$2\hat{\alpha}_{11} + \alpha_{33} = \frac{15(C_{1111} - C_{1122})}{16\omega_\delta}, \quad \hat{\alpha}_{11} + 2\alpha_{12} = \frac{3(C_{1111} + 2C_{1122})}{16\omega_\delta}. \tag{35}$$

Writing the constants of the isotropic elastic material in terms of Young's modulus (E) and Poisson's ratio (ν), we have that

$$C_{1111} = \frac{E(1-\nu)}{(1+\nu)(1-2\nu)}, \quad C_{1122} = \frac{\nu E}{(1+\nu)(1-2\nu)}. \tag{36}$$

Substitution of (36) into (35), yields

$$2\hat{\alpha}_{11} + \alpha_{33} = \frac{15E}{16(1+\nu)\omega_\delta}, \quad \hat{\alpha}_{11} + 2\alpha_{12} = \frac{3E}{16(1-2\nu)\omega_\delta}. \tag{37}$$

Aguiar (2016) proposes a decomposition of the difference displacement quotient state at $\mathbf{x}_0 \in \mathcal{B}$, defined in (1.b), in the form

$$\underline{\mathbf{h}}\langle\boldsymbol{\xi}\rangle = \underline{\varphi}\langle\boldsymbol{\xi}\rangle\underline{\mathbf{e}}\langle\boldsymbol{\xi}\rangle + \underline{\mathbf{h}}_d\langle\boldsymbol{\xi}\rangle, \tag{38}$$

where $\underline{\varphi}$ is a scalar state that yields the radial component of $\underline{\mathbf{h}}\langle\boldsymbol{\xi}\rangle$ and $\underline{\mathbf{h}}_d$ is a vector state that satisfies $\underline{\mathbf{h}}_d\langle\boldsymbol{\xi}\rangle \cdot \underline{\mathbf{e}}\langle\boldsymbol{\xi}\rangle = 0$.

Substituting (38) into (18) and using the equalities $\underline{\mathbf{e}}\langle\boldsymbol{\xi}\rangle \cdot \underline{\mathbf{h}}_d\langle\boldsymbol{\xi}\rangle \equiv 0$, $\underline{\underline{\mathbf{e}}}\langle\boldsymbol{\xi},\boldsymbol{\eta}\rangle \cdot \underline{\mathbf{e}}\langle\boldsymbol{\xi}\rangle \equiv 0$

and $\underline{\underline{\mathbf{e}}}\langle\boldsymbol{\xi},\boldsymbol{\eta}\rangle \cdot \underline{\mathbf{h}}_d\langle\boldsymbol{\xi}\rangle = \underline{\mathbf{e}}\langle\boldsymbol{\eta}\rangle \cdot \underline{\mathbf{h}}_d\langle\boldsymbol{\xi}\rangle / \sin\alpha$, we get the alternative form

$$\widehat{W}_{\mathbf{x}_0}[\underline{\mathbf{h}}] = \widehat{W}_{\mathbf{x}_0}[\underline{\varphi}\underline{\mathbf{e}}] + \widehat{W}_{\mathbf{x}_0}[\underline{\mathbf{h}}_d] + \frac{\hat{\alpha}_{13}}{2}\int_{N_\delta} \underline{\mathbf{h}}_d\langle\boldsymbol{\xi}\rangle \cdot \int_{N_\delta} \frac{\omega(|\boldsymbol{\xi}|,|\boldsymbol{\eta}|)}{sin\alpha}(\underline{\varphi}\langle\boldsymbol{\xi}\rangle + \underline{\varphi}\langle\boldsymbol{\eta}\rangle)\underline{\mathbf{e}}\langle\boldsymbol{\eta}\rangle dv_\eta dv_\xi, \quad (39)$$

where it follows from (18) that

$$\widehat{W}_{\mathbf{x}_0}[\underline{\varphi}\underline{\mathbf{e}}] = \frac{1}{2}\int_{N_\delta} \underline{\varphi}\langle\boldsymbol{\xi}\rangle \cdot \int_{N_\delta} \omega(|\boldsymbol{\xi}|,|\boldsymbol{\eta}|)[\hat{\alpha}_{11}\underline{\varphi}\langle\boldsymbol{\xi}\rangle + 2\alpha_{12}\underline{\varphi}\langle\boldsymbol{\eta}\rangle]dv_\eta dv_\xi, \quad (40)$$

$$\widehat{W}_{\mathbf{x}_0}[\underline{\mathbf{h}}_d] = \frac{\alpha_{33}}{4}\int_{N_\delta} \underline{\mathbf{h}}_d\langle\boldsymbol{\xi}\rangle \cdot \int_{N_\delta} \frac{\omega(|\boldsymbol{\xi}|,|\boldsymbol{\eta}|)}{(sin\alpha)^2}[\underline{\mathbf{e}}\langle\boldsymbol{\eta}\rangle \cdot \underline{\mathbf{h}}_d\langle\boldsymbol{\xi}\rangle + \underline{\mathbf{e}}\langle\boldsymbol{\xi}\rangle \cdot \underline{\mathbf{h}}_d\langle\boldsymbol{\eta}\rangle]\underline{\mathbf{e}}\langle\boldsymbol{\eta}\rangle dv_\eta dv_\xi. \quad (41)$$

Substituting (39)-(41) into (16), we obtain

$$\begin{aligned}\widehat{\mathbf{L}}_{\mathbf{x}_0}[\underline{\mathbf{h}}]\langle\boldsymbol{\xi}\rangle = \int_{N_\delta} \frac{\omega(|\boldsymbol{\xi}|,|\boldsymbol{\eta}|)}{|\boldsymbol{\xi}|}\{&\hat{\alpha}_{11}\underline{\varphi}\langle\boldsymbol{\xi}\rangle\underline{\mathbf{e}}\langle\boldsymbol{\xi}\rangle + 2\alpha_{12}\underline{\varphi}\langle\boldsymbol{\eta}\rangle\underline{\mathbf{e}}\langle\boldsymbol{\xi}\rangle \\ &+ \frac{\alpha_{33}}{2sin\alpha}(\underline{\mathbf{e}}\langle\boldsymbol{\eta}\rangle \cdot \underline{\mathbf{h}}_d\langle\boldsymbol{\xi}\rangle + \underline{\mathbf{e}}\langle\boldsymbol{\xi}\rangle \cdot \underline{\mathbf{h}}_d\langle\boldsymbol{\eta}\rangle)\underline{\underline{\mathbf{e}}}\langle\boldsymbol{\xi},\boldsymbol{\eta}\rangle \\ &+ \frac{\hat{\alpha}_{13}}{2sin\alpha}[(\underline{\varphi}\langle\boldsymbol{\xi}\rangle + \underline{\varphi}\langle\boldsymbol{\eta}\rangle)\underline{\underline{\mathbf{e}}}\langle\boldsymbol{\xi},\boldsymbol{\eta}\rangle \\ &+ \frac{1}{sin\alpha}(\underline{\mathbf{e}}\langle\boldsymbol{\eta}\rangle \cdot \underline{\mathbf{h}}_d\langle\boldsymbol{\xi}\rangle + \underline{\mathbf{e}}\langle\boldsymbol{\xi}\rangle \cdot \underline{\mathbf{h}}_d\langle\boldsymbol{\eta}\rangle)\underline{\mathbf{e}}\langle\boldsymbol{\xi}\rangle]\}dv_\eta.\end{aligned} \quad (42)$$

Aguiar (2016) shows that, near the natural state, the free energy function proposed by Silling et al. (2007) for a simple elastic peridynamic material can be approximated by

$$\underline{\widetilde{\mathbf{W}}}_{\mathbf{x}_0}[\underline{\mathbf{h}}] := \frac{\tilde{\kappa}\overline{\vartheta}[\underline{\varphi}]^2}{2} + \frac{\tilde{\alpha}}{2}\int_{N_\delta} \tilde{\omega}(|\boldsymbol{\xi}|)|\boldsymbol{\xi}|^2\left(\underline{\varphi}\langle\boldsymbol{\xi}\rangle - \frac{\overline{\vartheta}[\underline{\varphi}]}{3}\right)^2 dv_{\boldsymbol{\xi}}, \quad (43)$$

where $\tilde{\omega} : \mathbb{R} \to \mathbb{R}$ is a known weighting function, $\tilde{\kappa}$ and $\tilde{\alpha}$ are peridynamic material constants, and

$$m := \int_{N_\delta} \tilde{\omega}(|\boldsymbol{\xi}|)|\boldsymbol{\xi}|^2 dv_{\boldsymbol{\xi}}, \quad \overline{\vartheta}[\underline{\varphi}] := \frac{3}{m}\int_{N_\delta} \tilde{\omega}(|\boldsymbol{\xi}|)|\boldsymbol{\xi}|^2\underline{\varphi}\langle\boldsymbol{\xi}\rangle dv_{\boldsymbol{\xi}}. \quad (44)$$

Notice from (6) together with (38) that $\underline{\varepsilon}\langle\boldsymbol{\xi}\rangle \equiv \underline{\varphi}\langle\boldsymbol{\xi}\rangle$ and that, therefore, (44.b) is a weighted average of the infinitesimal normal strain in a δ-neighborhood of $\mathbf{x}_0$. It follows from (43) and (44.b) that distortions caused by angle changes between bonds are not considered in the energy function proposed by Silling et al. (2007) near the natural state.

The linearized force response function state, obtained from (16) together with (43)

and (44), is given by

$$\underline{\widetilde{\mathbf{L}}}_{\mathbf{x}_0}[\underline{\mathbf{h}}]\langle\boldsymbol{\xi}\rangle = \tilde{\omega}(|\boldsymbol{\xi}|)|\boldsymbol{\xi}| \left[\left(\tilde{\kappa} - \frac{\tilde{\alpha}m}{3^2}\right)\frac{3}{m}\overline{\vartheta}[\underline{\varphi}] + \tilde{\alpha}\underline{\varphi}\langle\boldsymbol{\xi}\rangle\right]\underline{\mathbf{e}}\langle\boldsymbol{\xi}\rangle. \tag{45}$$

Comparing (42) with (45), it is observed that the expressions are equivalent if

$$\hat{\alpha}_{11} = \frac{\tilde{\alpha}}{m}, \quad 2\alpha_{12} = \left(\frac{3}{m}\right)^2\tilde{\kappa} - \frac{\tilde{\alpha}}{m}, \quad \alpha_{33} = \hat{\alpha}_{13} = 0,$$

and

$$\omega(|\boldsymbol{\xi}|, |\boldsymbol{\eta}|) = \widetilde{\omega}(|\boldsymbol{\xi}|)\widetilde{\omega}(|\boldsymbol{\eta}|)|\boldsymbol{\xi}|^2|\boldsymbol{\eta}|^2. \tag{46}$$

Thus, the linearized model proposed by Silling et al. (2007) is a particular case of the linear model proposed by Aguiar e Fosdick (2014).

The two relations in (37) were obtained considering a homogeneous deformation. To obtain a third relation, Aguiar (2016) introduces a correspondence argument according to which the free energy function of the peridynamic material at $\mathbf{x}_0$ near the natural state is equal to the weighted average of the strain energy density function from classical elasticity theory in a δ-neighborhood of $\mathbf{x}_0$. Considering that (46) holds, the correspondence argument yields

$$\widehat{W}_{\mathbf{x}_0}[\underline{\mathbf{h}}] = \overline{W}^L_{\mathbf{x}_0}[\underline{\mathbf{h}}] := \frac{1}{m}\int_{N_\delta}\widetilde{\omega}(|\boldsymbol{\xi}|)\,|\boldsymbol{\xi}|^2\,\widehat{W}^L_{\mathbf{x}_0}[\widehat{\mathbf{E}}[\underline{\mathbf{h}}]]dv_\xi, \tag{47}$$

where $\widehat{\mathbf{E}}[\underline{\mathbf{h}}]$ is the infinitesimal strain tensor obtained from the vector state $\underline{\mathbf{h}}$ and m is given by (44.a). Observe from (47) with $\widehat{\mathbf{E}}[\underline{\mathbf{h}}]$ constant that $\widehat{W}_{\mathbf{x}_0}[\underline{\mathbf{h}}] = \widehat{W}^L_{\mathbf{x}_0}[\underline{\mathbf{h}}]$. Therefore, (25) with its left-hand side replaced by the strain energy function for an isotropic material of classical elasticity, which is given by

$$\widehat{W}^L_{\mathbf{x}_0}[\mathbf{E}] = \frac{1}{2}[\lambda(tr\mathbf{E})^2 + 2\mu\mathbf{E}\cdot\mathbf{E}], \tag{48}$$

and $\omega(\cdot,\cdot)$ given by (46) is a particular case of (47).

Using the decomposition (38), we search for a smooth deformation satisfying $\underline{\varphi}\langle\boldsymbol{\xi}\rangle = 0$, so that $\underline{\mathbf{h}} \equiv \underline{\mathbf{h}}_d$. In this case, (39) becomes $\widehat{W}_{\mathbf{x}_0}[\underline{\mathbf{h}}] \equiv \widehat{W}_{\mathbf{x}_0}[\underline{\mathbf{h}}_d]$. It follows from (47)

together with (41) that

$$\alpha_{33} = \frac{4\overline{W}^{L}_{\mathbf{x}_0}[\underline{\mathbf{h}}_d]}{\widehat{\Omega}_{\mathbf{x}_0}[\underline{\mathbf{h}}_d]}, \tag{49}$$

where

$$\widehat{\Omega}_{\mathbf{x}_0}[\underline{\mathbf{h}}_d] := \int_{N_\delta} \widetilde{\omega}(|\boldsymbol{\xi}|)\,|\boldsymbol{\xi}|^2\,\underline{\mathbf{h}}_d\langle\boldsymbol{\xi}\rangle \cdot \int_{N_\delta} \frac{\widetilde{\omega}(|\boldsymbol{\eta}|)\,|\boldsymbol{\eta}|^2}{(sin\alpha)^2}[\underline{\mathbf{e}}\langle\boldsymbol{\eta}\rangle \cdot \underline{\mathbf{h}}_d\langle\boldsymbol{\xi}\rangle + \underline{\mathbf{e}}\langle\boldsymbol{\xi}\rangle \cdot \underline{\mathbf{h}}_d\langle\boldsymbol{\eta}\rangle]\underline{\mathbf{e}}\langle\boldsymbol{\eta}\rangle dv_\eta dv_\xi. \tag{50}$$

To obtain α_{33} we need to consider a simple experiment that yields $\underline{\varphi}\langle\boldsymbol{\xi}\rangle \equiv 0$ for all bonds. The simple experiment consists of the torsion of a finite circular shaft in equilibrium, with no body force and subjected to a pair of couples applied to its ends, represented in Fig. 3. In classical linear elasticity, the solution of the problem is given by

$$\underline{\mathbf{u}}(\xi_1, \xi_2, \xi_3) = \beta\xi_3(-\xi_2\mathbf{e}_1 + \xi_1\mathbf{e}_2). \tag{51}$$

where β is the angle of twist per unit length of the shaft in its natural state, (ξ_1, ξ_2, ξ_3) are Cartesian coordinates with origin at a point $\mathbf{x}_0$ on the axis of the shaft, which is aligned with the ξ_3-direction, and $\{\mathbf{e}_1, \mathbf{e}_2, \mathbf{e}_3\}$ is the associated orthonormal basis, which is fixed.

Figure 3: Torsion of a finite circular shaft by a pair of couples applied to its ends.

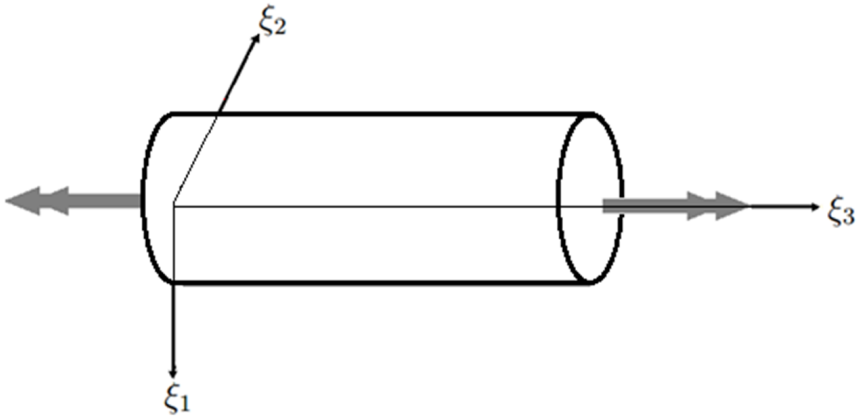

Source: Own author.

The non-zero components of the corresponding infinitesimal strain tensor $\mathbf{E}$ are

$$\epsilon_{13} = -\frac{\beta}{2}\xi_2, \quad \epsilon_{23} = -\frac{\beta}{2}\xi_1.$$

Substituting $\widehat{\mathbf{E}}[\underline{\mathbf{h}}] \equiv \mathbf{E}(\xi_1, \xi_2, \xi_3)$) into the right-hand side of (47), together with

the expression (48) and the transformations

$$\xi_1 = \rho\ cos\theta\ sin\phi, \xi_2 = \rho\ sin\theta\ sin\phi, \xi_3 = \rho\ cos\phi, \tag{52}$$

and taking the limits of integration given by (33), we arrive at

$$\overline{W}^L_{\mathbf{x}_0}[\underline{\mathbf{h}}] = \frac{\beta^2\mu\ m_6}{3m}, \quad m_n := 4\pi \int_0^\delta \widetilde{\omega}(\rho)\rho^n d\rho. \tag{53}$$

Since $|\boldsymbol{\xi}| = \rho$ in a δ-neighborhood of $\mathbf{x}_0$ and in view of both (51) and (52), we obtain

$$\underline{\mathbf{h}}\langle\boldsymbol{\xi}\rangle = \frac{\mathbf{u}(\rho,\phi,\theta)}{\rho} = \frac{\beta}{2}\rho\ 2\phi\ \mathbf{e}_\theta, \tag{54}$$

where $\{\mathbf{e}_\rho, \mathbf{e}_\phi, \mathbf{e}_\theta\}$ is the associated orthonormal basis for the spherical coordinate system with origin at $\mathbf{x}_0$, that is related to $\{\mathbf{e}_1, \mathbf{e}_2, \mathbf{e}_3\}$ by

$$\begin{aligned} \mathbf{e}_1 &= cos\theta\, sin\phi\, \mathbf{e}_\rho + cos\theta\, cos\phi\, \mathbf{e}_\phi - sin\theta\, \mathbf{e}_\theta, \\ \mathbf{e}_2 &= sin\theta\, sin\phi\, \mathbf{e}_\rho + sin\theta\, cos\phi\, \mathbf{e}_\phi + cos\theta\, \mathbf{e}_\theta, \quad \mathbf{e}_3 = cos\phi\, \mathbf{e}_\rho + sin\phi\, \mathbf{e}_\phi. \end{aligned} \tag{55}$$

It follows from (38) that $\underline{\varphi}\langle\boldsymbol{\xi}\rangle = \underline{\mathbf{h}}\langle\boldsymbol{\xi}\rangle \cdot \underline{\mathbf{e}}\langle\boldsymbol{\xi}\rangle \equiv 0$. Substituting (54) into (50) and using the limits of integration in (33), we obtain

$$\widehat{\Omega}_{\mathbf{x}_0}[\underline{\mathbf{h}}_d] = \frac{\beta^2 m m_6}{15}. \tag{56}$$

Substituting (53.a) and (56) into (49), we then get

$$\alpha_{33} = \frac{20\mu}{m^2}. \tag{57}$$

Substituting (57) and the expressions $\mu = E/(2(1+\nu))$ and $\kappa = E/(3(1-2\nu))$ into (37), we obtain the two other constants, which are given by

$$\hat{\alpha}_{11} = \frac{5\mu}{m^2}, \quad \alpha_{12} = \frac{1}{2m^2}(9\kappa + 25\mu)\ . \tag{58}$$

In the next section we present a similar approach together with a different experiment to evaluate the remaining perydinamic constant, $\hat{\alpha}_{13}$. This evaluation represents an original contribution of this work.

4 DETERMINATION OF FOURTH PERIDYNAMIC CONSTANT

In this chapter we use a fixed orthonormal basis $\{\mathbf{e}_1, \mathbf{e}_2, \mathbf{e}_3\}$ associated to the Cartesian coordinates (ξ_1, ξ_2, ξ_3) with origin at the centroid of the left end of the beam or shaft, which is aligned with the ξ_3-direction. We use to calculate the numerical integrations in Sections 4.2, 4.3 and 4.4 the software MATHEMATICA 9 © through global adaptive strategy.

4.1 Pure bending experiment

The determination of the constant $\hat{\alpha}_{13}$ is one of the objectives of this work. This constant represents nonlocal effects of the peridynamic material and can not be determined from the approach leading to expressions in (37). To determinate $\hat{\alpha}_{13}$, we use a simple experiment in mechanics that provides a deformation field for which both radial and non-radial components of $\underline{\mathbf{h}}$ in (38) do not vanish.

Figure 4: Beam bent by terminal couples.

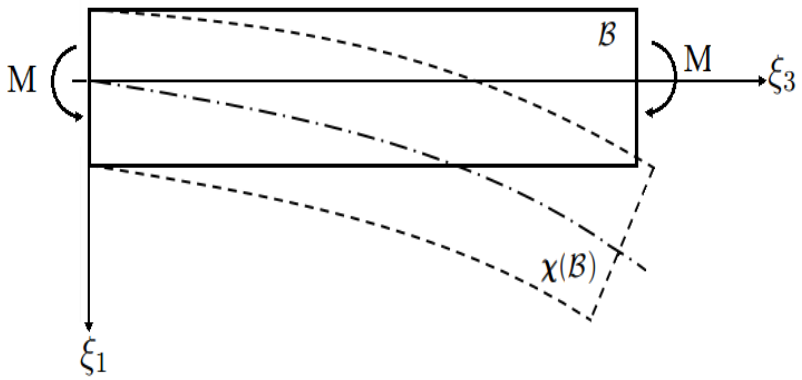

Source: Own author

The experiment consists of a beam bent by terminal couples with no body forces acting, as illustrated in Fig. 4. In classical linear elasticity, the resulting displacement field of this problem is given by (SOKOLNIKOFF, 1956)

$$\mathbf{u}(\xi_1, \xi_2, \xi_3) = \frac{M}{2EI}[({\xi_3}^2 + \nu{\xi_1}^2 - \nu{\xi_2}^2)\mathbf{e}_1 + 2\nu\xi_1\xi_2\mathbf{e}_2 - 2\xi_1\xi_3\mathbf{e}_3], \tag{59}$$

where M is the resulting moment applied at the ends of the beam, which is taken to be positive, I is the moment of inertia with respect to the ξ_2-direction, and we recall from Section 3.2 that ν is the Poisson's ratio and E is the Young's modulus. The solution (59)

was reached by fixing the centroid of the left end of the beam at the origin and by fixing an element of the ξ_3-axis and an element of the $\xi_1\,\xi_3$-plane at the origin. The non-zero components of the corresponding infinitesimal strain tensor $\mathbf{E}$ are given by

$$\epsilon_{11} = \epsilon_{22} = \frac{M}{EI}\nu\xi_1, \quad \epsilon_{33} = -\frac{M}{EI}\xi_1. \tag{60}$$

4.2 Determination of the constant $\hat{\alpha}_{13}$

To apply the correspondence argument presented in the last chapter, which yields the expression (47), first, we use (48) together with $\widehat{\mathbf{E}}[\underline{\mathbf{h}}] \equiv \mathbf{E}(\xi_1, \xi_2, \xi_3)$ and the strain components given by (60) to obtain $\widehat{W}^L_{\mathbf{x}_0}[\widehat{\mathbf{E}}[\underline{\mathbf{h}}]] = (M^2/2EI^2)\xi_1^2$. Using the transformations (52) and taking the limits of integration in (33), we obtain

$$\overline{W}^L_{\mathbf{x}_0}[\underline{\mathbf{h}}] = \frac{M^2 m_6}{6EI^2 m}, \tag{61}$$

where $m = m_4$ and m_6 are given by (53.b).

Using the expression $\underline{\mathbf{h}}\langle\boldsymbol{\xi}\rangle = \mathbf{u}(\rho, \phi, \theta)/\rho$, the decomposition (38), and the transformation (52) and (55) from the cartesian coordinate system to the spherical coordinate system, we get the radial and non-radial components, given by, respectively,

$$\underline{\varphi}\langle\boldsymbol{\xi}\rangle = \frac{M\rho}{2EI} cos\theta\ sin\phi(\nu^2\phi - cos^2\phi), \tag{62}$$

$$\underline{\mathbf{h}}_d\langle\boldsymbol{\xi}\rangle = \frac{M\rho}{4EI}\{-cos\phi\ cos\theta[-3-\nu+(1+\nu)cos(2\phi)]\mathbf{e}_\phi + 2sin\theta(\nu^2\phi - cos^2\phi)\mathbf{e}_\theta\}.$$

Using the relation (46), we rewrite (39) along with (40) and (41) in the form

$$\begin{aligned}\widehat{W}_{\mathbf{x}_0}[\underline{\mathbf{h}}] =& \hat{\alpha}_{11}\widehat{A}_{\mathbf{x}_0}[\underline{\mathbf{h}}]_{11} + \alpha_{12}\widehat{A}_{\mathbf{x}_0}[\underline{\mathbf{h}}]_{12} + \\ & \alpha_{33}(\widehat{A}_{\mathbf{x}_0}[\underline{\mathbf{h}}]_{33} + \widehat{B}_{\mathbf{x}_0}[\underline{\mathbf{h}}]_{33}) + \hat{\alpha}_{13}(\widehat{A}_{\mathbf{x}_0}[\underline{\mathbf{h}}]_{13} + \widehat{B}_{\mathbf{x}_0}[\underline{\mathbf{h}}]_{13}),\end{aligned} \tag{63}$$

where

$$\begin{aligned}\widehat{A}_{\mathbf{x}_0}[\underline{\mathbf{h}}]_{11} &:= \frac{1}{2}\int_{N_\delta} \widetilde{\omega}(|\boldsymbol{\xi}|)\,|\boldsymbol{\xi}|^2\,\underline{\varphi}\langle\boldsymbol{\xi}\rangle^2 \int_{N_\delta} \widetilde{\omega}(|\boldsymbol{\eta}|)\,|\boldsymbol{\eta}|^2\,dv_\eta dv_\xi, \\ \widehat{A}_{\mathbf{x}_0}[\underline{\mathbf{h}}]_{12} &:= \int_{N_\delta} \widetilde{\omega}(|\boldsymbol{\xi}|)\,|\boldsymbol{\xi}|^2\,\underline{\varphi}\langle\boldsymbol{\xi}\rangle \int_{N_\delta} \widetilde{\omega}(|\boldsymbol{\eta}|)\,|\boldsymbol{\eta}|^2\,\underline{\varphi}\langle\boldsymbol{\eta}\rangle dv_\eta dv_\xi, \\ \widehat{A}_{\mathbf{x}_0}[\underline{\mathbf{h}}]_{33} &:= \frac{1}{4}\int_{N_\delta} \widetilde{\omega}(|\boldsymbol{\xi}|)\,|\boldsymbol{\xi}|^2\,\underline{\mathbf{h}}_d\langle\boldsymbol{\xi}\rangle \cdot \int_{N_\delta} \frac{\widetilde{\omega}(|\boldsymbol{\eta}|)\,|\boldsymbol{\eta}|^2}{(sin\alpha)^2}(\underline{\mathbf{e}}\langle\boldsymbol{\eta}\rangle \cdot \underline{\mathbf{h}}_d\langle\boldsymbol{\xi}\rangle)\underline{\mathbf{e}}\langle\boldsymbol{\eta}\rangle dv_\eta dv_\xi,\end{aligned} \tag{64}$$

$$\widehat{B}_{\mathbf{x}_0}[\underline{\mathbf{h}}]_{33} := \frac{1}{4}\int_{N_\delta} \widetilde{\omega}(|\boldsymbol{\xi}|)\,|\boldsymbol{\xi}|^2\,\underline{\mathbf{h}}_d\langle\boldsymbol{\xi}\rangle \cdot \int_{N_\delta} \frac{\widetilde{\omega}(|\boldsymbol{\eta}|)\,|\boldsymbol{\eta}|^2}{(sin\alpha)^2}(\underline{\mathbf{e}}\langle\boldsymbol{\xi}\rangle \cdot \underline{\mathbf{h}}_d\langle\boldsymbol{\eta}\rangle)\underline{\mathbf{e}}\langle\boldsymbol{\eta}\rangle dv_\eta dv_\xi,$$

$$\widehat{A}_{\mathbf{x}_0}[\underline{\mathbf{h}}]_{13} := \frac{1}{2}\int_{N_\delta} \widetilde{\omega}(|\boldsymbol{\xi}|)\,|\boldsymbol{\xi}|^2\,\underline{\mathbf{h}}_d\langle\boldsymbol{\xi}\rangle \cdot \int_{N_\delta} \frac{\widetilde{\omega}(|\boldsymbol{\eta}|)\,|\boldsymbol{\eta}|^2}{sin\alpha}(\underline{\varphi}\langle\boldsymbol{\xi}\rangle)\underline{\mathbf{e}}\langle\boldsymbol{\eta}\rangle dv_\eta dv_\xi,$$

$$\widehat{B}_{\mathbf{x}_0}[\underline{\mathbf{h}}]_{13} := \frac{1}{2}\int_{N_\delta} \widetilde{\omega}(|\boldsymbol{\xi}|)\,|\boldsymbol{\xi}|^2\,\underline{\mathbf{h}}_d\langle\boldsymbol{\xi}\rangle \cdot \int_{N_\delta} \frac{\widetilde{\omega}(|\boldsymbol{\eta}|)\,|\boldsymbol{\eta}|^2}{sin\alpha}(\underline{\varphi}\langle\boldsymbol{\eta}\rangle)\underline{\mathbf{e}}\langle\boldsymbol{\eta}\rangle dv_\eta dv_\xi.$$

Next, using (62) and the limits of integration in (33) in the first two expressions of (64), we get

$$\widehat{A}_{\mathbf{x}_0}[\underline{\mathbf{h}}]_{11} = \frac{mm_6}{840}\frac{M^2}{(EI)^2}(24\nu^2 - 8\nu + 3), \qquad \widehat{A}_{\mathbf{x}_0}[\underline{\mathbf{h}}]_{12} = 0. \tag{65}$$

The integrals in the other four expressions in (64) are evaluated numerically. Each one of them was divided in three parts that multiply either 1, ν, or, ν^2. The values obtained from numerical integration converge to rational numbers multiplied by π^2, or, π^3. The four resulting expressions are then given by

$$\begin{aligned} &\widehat{A}_{\mathbf{x}_0}[\underline{\mathbf{h}}]_{33} = \frac{mm_6}{6720}\frac{M^2}{(EI)^2}(64\nu^2 + 16\nu + 92), \qquad \widehat{B}_{\mathbf{x}_0}[\underline{\mathbf{h}}]_{33} = 0, \\ &\widehat{A}_{\mathbf{x}_0}[\underline{\mathbf{h}}]_{13} = 0, \qquad \widehat{B}_{\mathbf{x}_0}[\underline{\mathbf{h}}]_{13} = \frac{\pi {m_5}^2}{3360}\frac{M^2}{(EI)^2}(-11\nu^2 + 20\nu - 4). \end{aligned} \tag{66}$$

Substituting the expresions in (65) and (66) back into (63) and equating the resulting expression to (61), we finally get that

$$\hat{\alpha}_{13} = \frac{140}{\pi}\frac{m_6}{m}\frac{\mu}{m_5^2}\frac{8\nu^2 - 8\nu - 1}{11\nu^2 - 20\nu + 4}. \tag{67}$$

The expression (67) was obtained by evaluating the free energy function at the origin of the coordinate system, that is, at the center of the left end of the beam. Below we will calculate the peridynamic free energy function and the classical strain energy density for an arbitrary point, replacing the peridynamic constants with the corresponding expressions (57), (58) and (67), and verify if the correspondence argument is satisfied.

To obtain the infinitesimal strain tensor $\mathbf{E}$ evaluated at $\mathbf{x}_0 = (x_0,\, y_0,\, z_0)$, we substitute

$$\xi_1 = \widehat{\xi}_1 + x_0,\ \xi_2 = \widehat{\xi}_2 + y_0 \ \text{ and } \ \xi_3 = \widehat{\xi}_3 + z_0 \tag{68}$$

into the expressions (60), where $(\widehat{\xi}_1, \widehat{\xi}_2, \widehat{\xi}_3)$ are the components of the relative position

vector $\boldsymbol{\xi}$. Using the transformations

$$\widehat{\xi}_1 = \rho\ cos\theta\, sin\phi, \quad \widehat{\xi}_2 = \rho\ sin\theta\ sin\phi, \quad \widehat{\xi}_3 = \rho\ cos\phi, \tag{69}$$

and taking the limits of integration in (33), we obtain

$$\overline{W}^L_{\mathbf{x}_0}[\underline{\mathbf{h}}] = \frac{M^2}{EI^2}\left(\frac{{x_0}^2}{2} + \frac{m_6}{6m}\right), \tag{70}$$

where $m = m_4$ and m_6 are given by (53.b). We can observe from (70) that only the first term within parentheses depends upon the position $\mathbf{x}_0$ and the remaining term yields (61).

Now we want to calculate the peridynamic free energy function to compare it with the weighted average of the strain energy density function (70). The difference displacement state $\underline{\mathbf{u}}$ is, by definition, given by

$$\underline{\mathbf{u}}\langle\boldsymbol{\xi}\rangle := (\mathbf{u}(\mathbf{x}) - \mathbf{u}(\mathbf{x}_0))\ |_{\mathbf{x}=\mathbf{x}_0+\boldsymbol{\xi}}, \tag{71}$$

where the displacemente field $\mathbf{u}(\mathbf{x})$ is given by (59). Using (1.b) we then obtain the displacement quotient state

$$\begin{aligned}\underline{\mathbf{h}}\langle\boldsymbol{\xi}\rangle =& \frac{M}{2EI\,|\boldsymbol{\xi}|}\Big(\left\{\widehat{\xi}_3\,(2z_0 + \widehat{\xi}_3) + \nu\left[\widehat{\xi}_1^2 + 2z_0\,\widehat{\xi}_1 - \widehat{\xi}_2\,(2y_0 + \widehat{\xi}_2)\right]\right\}\mathbf{e}_1 \\ &+ 2\nu\left[y_0\,\widehat{\xi}_1 + (x_0 + \widehat{\xi}_1)\widehat{\xi}_2\right]\mathbf{e}_2 - 2\left[z_0\widehat{\xi}_1 + (x_0 + \widehat{\xi}_1)\widehat{\xi}_3\right]\mathbf{e}_3\Big).\end{aligned} \tag{72}$$

Recall from the decomposition (38) that

$$\underline{\varphi}\langle\boldsymbol{\xi}\rangle = \underline{\mathbf{h}}\langle\boldsymbol{\xi}\rangle \cdot \underline{\mathbf{e}}\langle\boldsymbol{\xi}\rangle \ \text{ and } \ \underline{\mathbf{h}}_d\langle\boldsymbol{\xi}\rangle = \underline{\mathbf{h}}\langle\boldsymbol{\xi}\rangle - \underline{\varphi}\langle\boldsymbol{\xi}\rangle\underline{\mathbf{e}}\langle\boldsymbol{\xi}\rangle, \tag{73}$$

where $\underline{\mathbf{e}}$ is given by (2). Here, we have that $\underline{\mathbf{e}}\langle\boldsymbol{\xi}\rangle = \xi_1\,\mathbf{e}_1 + \xi_2\,\mathbf{e}_2 + \xi_3\,\mathbf{e}_3$. Substituting this expression together with (72) into (73) and using the coordinate transformations in (69) we obtain expressions for $\underline{\varphi}\langle\boldsymbol{\xi}\rangle$ and $\underline{\mathbf{h}}_d\langle\boldsymbol{\xi}\rangle$ that can be substituted inside the integrals (39), (40) and (41). With the limits of integration (33), the expression (40) becomes

$$\begin{aligned}\widehat{W}_{\mathbf{x}_0}[\underline{\varphi}\,\underline{\mathbf{e}}] =& \frac{\hat{\alpha}_{11}}{2}\left(\frac{M}{EI}\right)^2\left[m^2\frac{1}{15}(3 - 4\nu + 8\nu^2){x_0}^2 + m_6\,m\,\frac{3 - 8\nu + 24\nu^2}{420}\right] \\ &+ \alpha_{12}\left(\frac{M}{EI}\right)^2\frac{m^2}{9}(1 - 2\nu)^2{x_0}^2.\end{aligned} \tag{74}$$

We can observe from (74) that the second term inside the brackets yields $\widehat{A}_{\mathbf{x}_0}[\underline{\mathbf{h}}]_{11}$ in (65.a), and the remaining terms are position dependent and proportional to ${x_0}^2$.

To solve the integrals that multiply $\hat{\alpha}_{13}$ and α_{33} in (39) and (41), respectively, we need to use numerical integration. We divide the integrands into 10 parts that multiply 1, x_0, y_0, z_0, ${x_0}^2$, ${y_0}^2$, ${z_0}^2$, $x_0\,y_0$, $x_0\,z_0$, and $y_0\,z_0$. Then, we divide again the terms that multiply 1, ν, and ν^2, and finally integrate numerically each one of these parts.

Concerning the integrals that multiply $\hat{\alpha}_{13}$, the ones that also multiply terms in the set $\{x_0,\, y_0,\, z_0,\, {x_0}^2,\, {y_0}^2,\, {z_0}^2,\, x_0\,y_0,\, x_0\,z_0,\, y_0\,z_0\}$ are nearly zero when compare to the remaining three integrals that multiply 1. These integrals yield the expression of $\widehat{B}_{\mathbf{x}_0}[\underline{\mathbf{h}}]_{13}$ presented in (66.b). Using these results, integral in (39) becomes

$$\widehat{W}_{\mathbf{x}_0}[\underline{\mathbf{h}}] = \widehat{W}_{\mathbf{x}_0}[\underline{\varphi}\underline{\mathbf{e}}] + \widehat{W}_{\mathbf{x}_0}[\underline{\mathbf{h}}_d] + \frac{\hat{\alpha}_{13}}{2}\frac{\pi {m_5}^2}{32}\frac{M^2}{(EI)^2}\frac{(-11\nu^2+20\nu-4)}{105}. \tag{75}$$

Among the integrals that multiply α_{33}, in addition to the position independent terms, also the terms that multiply ${x_0}^2$ do not vanish. A procedure similar to the one presented above yields

$$\widehat{W}_{\mathbf{x}_0}[\underline{\mathbf{h}}_d] = \alpha_{33}\frac{M^2}{(EI)^2}\left[m^2\,(1+\nu)^2\frac{{x_0}^2}{45} + \frac{m\,m_6}{64}\frac{(64\nu^2+16\nu+92)}{105}\right]. \tag{76}$$

Replacing (74) and (76) into (75) and using the expressions (57), (58) and (67) for the peridynamic constants, we finally obtain

$$\widehat{W}_{\mathbf{x}_0}[\underline{\mathbf{h}}] = \frac{M^2}{EI^2}\left(\frac{{x_0}^2}{2} + \frac{m_6}{6m}\right). \tag{77}$$

We can see from (70) and (77) that the free energy function is equal to the weighted average of the strain energy density function at any point $\mathbf{x}_0$ when we consider the displacement field for pure bending experiment and the expressions (57), (58) and (67) for the peridynamic constants.

In the next two sections we use different experiments to independently verify the correspondence argument, given by (47), when we use the expressions (57), (58) and (67) for the peridynamic constants.

4.3 Bending by terminal loads experiment

The expressions (57) and (58) were obtained by considering the experiment of uniform torsion of a circular shaft and (67) by considering a beam bent by terminal couples. To test if these values are valid, we consider two different experiments: a beam bent by terminal loads in this section and a circular shaft subjected to anti-plane shear in the next section.

Figure 5: Beam subjected to terminal load.

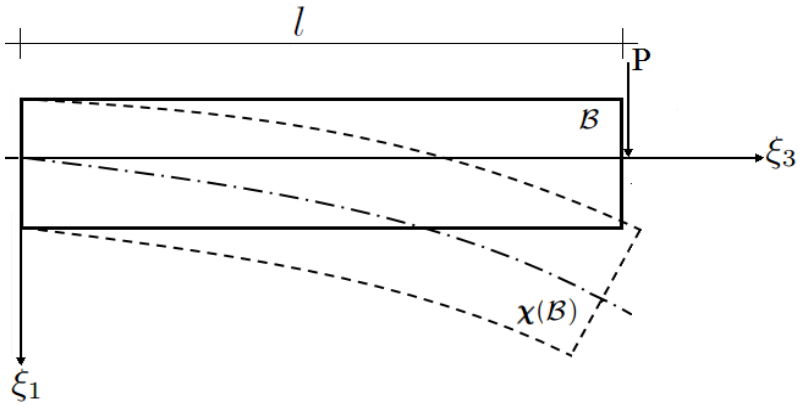

Source: Own author

The experiment of a beam subjected to terminal loads is illustrated in Fig. 5. Considering no body forces acting, and imposing the same restrictions described after the expression (59) the displacement field corresponding to this experiment is given, in classical linear elasticity, by (SOKOLNIKOFF, 1956)

$$\begin{aligned}\mathbf{u}(\xi_1,\xi_2,\xi_3) =& \frac{P}{EI}\Big[(\frac{1}{2}\nu(l-\xi_3)({\xi_1}^2-{\xi_2}^2)-\frac{1}{6}{\xi_3}^3+\frac{1}{2}l\,{\xi_2}^2)\mathbf{e}_1+\nu\,\xi_1\,\xi_2(l-\xi_3)\mathbf{e}_2 \\ &-\left(\Phi(\xi_1,\xi_2)+\xi_1{\xi_2}^2+(l\,\xi_3-\frac{1}{2}{\xi_3}^2)\xi_1\right)\mathbf{e}_3\Big],\end{aligned} \tag{78}$$

where l is the beam length, P is the load applied parallel to $\mathbf{e}_1$ at the right end, and $\Phi(\xi_1,\xi_2)$ is the classical Saint-Venant flexure function, which is harmonic, that is

$$\frac{\partial^2\Phi}{\partial{\xi_1}^2}+\frac{\partial^2\Phi}{\partial{\xi_2}^2}=0 \quad \text{on } \mathcal{B}. \tag{79}$$

For zero external force on the lateral surface Ω of the beam, Φ must satisfy

$$\frac{d\,\Phi}{d\mathbf{n}}=-\left[\frac{1}{2}\nu{\xi_1}^2+(1-\frac{1}{2}\nu){\xi_2}^2\right]cos(\xi_1,\mathbf{n})-(2+\nu)\xi_1\,\xi_2\,cos(\xi_2,\mathbf{n}) \qquad \text{on} \quad \Omega, \tag{80}$$

where $\mathbf{n}$ denotes the exterior unit normal vector to the boundary Ω.

The solution for the system of differential equations (79) and (80), when Ω is the lateral surface of a circular cylinder, is given by

$$\Phi(\xi_1, \xi_2) = \frac{1}{4}({\xi_1}^3 - 3\,\xi_1\,{\xi_2}^2) - a^2\,\xi_1(\frac{3}{4} + \frac{\nu}{2}), \tag{81}$$

where a is the radius of the cross section of the cylinder.

Replacing (81) into (78) and using the definition

$$\mathbf{E} := (\operatorname{grad}\mathbf{u} + \operatorname{grad}\mathbf{u}^T)/2, \tag{82}$$

the matrix form of the corresponding infinitesimal strain tensor $\mathbf{E}$ in the basis $\{\mathbf{e}_1, \mathbf{e}_2, \mathbf{e}_3\}$ is given by

$$[\mathbf{E}] = \frac{P}{EI}\begin{bmatrix} \nu\,\xi_1(l-\xi_3) & 0 & \frac{[(a^2-{\xi_1}^2)(3+2\nu)+(2\nu-1){\xi_2}^2]}{8} \\ 0 & \nu\,\xi_1(l-\xi_3) & -\frac{(1+2\nu)\xi_1\,\xi_2}{4} \\ \frac{[(a^2-{\xi_1}^2)(3+2\nu)+(2\nu-1){\xi_2}^2]}{8} & -\frac{(1+2\nu)\xi_1\,\xi_2}{4} & \xi_1(l-\xi_3) \end{bmatrix}. \tag{83}$$

We substitute (68) into (83) to calculate $\widehat{W}^L_{\mathbf{x}_0}[\widehat{\mathbf{E}}[\underline{\mathbf{h}}]]$ and use the transformations (69) together with the limits in (33) to calculate $\overline{W}^L_{\mathbf{x}_0}[\underline{\mathbf{h}}]$, both in (47). However, the resulting expression is rather long and will not be presented here. In the next pages we will get numerical values for this expression.

To evaluate the integrals of the free energy function given by (39)-(41), we start by getting $\underline{\mathbf{h}}\langle\boldsymbol{\xi}\rangle$ through the definitions (1.b) and (71) together with the displacement field (78). We then use (73) to get $\underline{\varphi}\langle\boldsymbol{\xi}\rangle$ and $\underline{\mathbf{h}_d}\langle\boldsymbol{\xi}\rangle$.

Substituting $\underline{\varphi}\langle\boldsymbol{\xi}\rangle$ and $\underline{\mathbf{h}_d}\langle\boldsymbol{\xi}\rangle$ into (39)-(41), the expressions obtained for the terms that multiply $\hat{\alpha}_{13}$ and α_{33} are extremely difficult to integrate. Therefore, from here on, we introduce numerical values for the mechanical properties of the material and the geometrical properties of the problem in order to obtain numerical values for the integrals. We remove two parameters from our calculations by dividing both sides of (47) by P^2/E^2. So, from here on, in this section, we use the transformations $\widehat{W}_{\mathbf{x}_0}[\underline{\mathbf{h}}] = \widehat{W}_{\mathbf{x}_0}[\underline{\mathbf{h}}]/(P^2/E^2)$ and $\overline{W}^L_{\mathbf{x}_0}[\underline{\mathbf{h}}] = \overline{W}^L_{\mathbf{x}_0}[\underline{\mathbf{h}}]/(P^2/E^2)$.

The mechanical properties used are

$$\nu = 0.25,\ \delta = 0.1\,a, \tag{84}$$

and the geometrical properties are

$$a = 1\,\text{Ul (unit of length)},\ l = 5\,a,\ I = \pi\,a^4/4. \tag{85}$$

Also, we consider that

$$\widetilde{\omega}(|\boldsymbol{\xi}|) = \frac{1}{|\boldsymbol{\xi}|^2}. \tag{86}$$

Moreover the free energy function and the strain energy density are calculated for a set of arbitrary points inside the domain, as explained below.

In Tab. 2, we have the result of the numerical integrations at nine different points. The parameters A_{11}, A_{12}, A_{33}, and A_{13} are the integrals that multiply $\hat{\alpha}_{11}$, α_{12}, α_{33}, and $\hat{\alpha}_{13}$, respectively, and have the following form

$$\begin{aligned}
A_{11} &:= \int_{N_\delta} \widetilde{\omega}(|\boldsymbol{\xi}|)\,|\boldsymbol{\xi}|^2\,\underline{\varphi}\langle\boldsymbol{\xi}\rangle^2 \int_{N_\delta} \widetilde{\omega}(|\boldsymbol{\eta}|)\,|\boldsymbol{\eta}|^2\,dv_\eta dv_\xi,\\
A_{12} &:= \int_{N_\delta} \widetilde{\omega}(|\boldsymbol{\xi}|)\,|\boldsymbol{\xi}|^2\,\underline{\varphi}\langle\boldsymbol{\xi}\rangle \int_{N_\delta} \widetilde{\omega}(|\boldsymbol{\eta}|)\,|\boldsymbol{\eta}|^2\,\underline{\varphi}\langle\boldsymbol{\eta}\rangle dv_\eta dv_\xi,\\
A_{33} &:= \int_{N_\delta} \widetilde{\omega}(|\boldsymbol{\xi}|)\,|\boldsymbol{\xi}|^2\,\underline{\mathbf{h}}_d\langle\boldsymbol{\xi}\rangle \cdot \int_{N_\delta} \frac{\widetilde{\omega}(|\boldsymbol{\eta}|)\,|\boldsymbol{\eta}|^2}{(sin\alpha)^2}(\underline{\mathbf{e}}\langle\boldsymbol{\eta}\rangle \cdot \underline{\mathbf{h}}_d\langle\boldsymbol{\xi}\rangle + \underline{\mathbf{e}}\langle\boldsymbol{\xi}\rangle \cdot \underline{\mathbf{h}}_d\langle\boldsymbol{\eta}\rangle)\underline{\mathbf{e}}\langle\boldsymbol{\eta}\rangle dv_\eta dv_\xi,\\
A_{13} &:= \int_{N_\delta} \widetilde{\omega}(|\boldsymbol{\xi}|)\,|\boldsymbol{\xi}|^2\,\underline{\mathbf{h}}_d\langle\boldsymbol{\xi}\rangle \cdot \int_{N_\delta} \frac{\widetilde{\omega}(|\boldsymbol{\eta}|)\,|\boldsymbol{\eta}|^2}{sin\alpha}(\underline{\varphi}\langle\boldsymbol{\xi}\rangle + \underline{\varphi}\langle\boldsymbol{\eta}\rangle)\underline{\mathbf{e}}\langle\boldsymbol{\eta}\rangle dv_\eta dv_\xi.
\end{aligned} \tag{87}$$

Using the values given in (84) and the expressions (57), (58) and (67), the numerical values for the peridynamic constants are $\hat{\alpha}_{11} \approx 113986$, $\alpha_{12} \approx 113986$, $\alpha_{33} \approx 455945$ and $\hat{\alpha}_{13} \approx 8669212$. In Tab. 3 we have these values multiplied by the values of Tab. 2 and, in the last two columns, the values of the free energy function and the weighted average of the strain energy density. Notice that the values at the sixth column $\widehat{W}_{\mathbf{x}_0}[\underline{\mathbf{h}}]$ are the sum of the four columns to its left hand side. Comparison between the two last columns shows that the correspondence argument (47) is approximately satisfied for the beam bent by terminal loads problem at the nine chosen points using the values given by (84) and (85).

The maximum percentage error between the two columns defined by

$$(\widehat{W}_{\mathbf{x}_0}[\underline{\mathbf{h}}] - \overline{W}^L_{\mathbf{x}_0}[\underline{\mathbf{h}}]) * 100/\overline{W}^L_{\mathbf{x}_0}[\underline{\mathbf{h}}] \tag{88}$$

is 0.18%, which is small, considering that because of the form of the integrals, the values from numerical integration are not highly accurate.

Table 2: Results of numerical integrations for the problem of the beam bent by terminal loads.

(x_0, y_0, z_0)	A_{11}	A_{12}	A_{33}	A_{13}
(0, 0, 0)	$1.47583 \cdot 10^{-6}$	0	$1.70017 \cdot 10^{-6}$	$2.36814 \cdot 10^{-9}$
(0.2, 0, 0)	$6.10305 \cdot 10^{-6}$	$7.90119 \cdot 10^{-7}$	$5.5376 \cdot 10^{-6}$	$2.34618 \cdot 10^{-9}$
(0.4, 0, 0)	$2.00126 \cdot 10^{-5}$	$3.16048 \cdot 10^{-6}$	$1.70792 \cdot 10^{-5}$	$2.87896 \cdot 10^{-9}$
(0.6, 0, 0)	$4.32881 \cdot 10^{-5}$	$7.11117 \cdot 10^{-6}$	$3.64024 \cdot 10^{-5}$	$2.61717 \cdot 10^{-9}$
(0.8, 0, 0)	$7.6069 \cdot 10^{-5}$	$1.26419 \cdot 10^{-5}$	$6.36532 \cdot 10^{-5}$	$2.86705 \cdot 10^{-9}$
(0, 0.4, 0)	$1.41031 \cdot 10^{-6}$	0	$1.63497 \cdot 10^{-6}$	$2.3393 \cdot 10^{-9}$
(0, 0, 2)	$1.45957 \cdot 10^{-6}$	0	$2.1033 \cdot 10^{-6}$	$7.11753 \cdot 10^{-10}$
(0.4, 0.4, 0)	$1.99851 \cdot 10^{-5}$	$3.16048 \cdot 10^{-6}$	$1.70503 \cdot 10^{-5}$	$2.45249 \cdot 10^{-9}$
(0.4, 0.4, 0.4)	$1.70685 \cdot 10^{-5}$	$2.67503 \cdot 10^{-6}$	$2.3794 \cdot 10^{-5}$	$2.0836 \cdot 10^{-9}$

Table 3: Terms of free energy function and strain energy density for the problem of the beam bent by terminal loads.

(x_0, y_0, z_0)	$A_{11} \cdot \hat{\alpha}_{11}/2$	$A_{12} \cdot \alpha_{12}$	$A_{33} \cdot \alpha_{33}/4$	$A_{13} \cdot \hat{\alpha}_{13}/2$	$\widehat{W}_{\mathbf{x}_0}[\underline{\mathbf{h}}]$	$\overline{W}^L_{\mathbf{x}_0}[\underline{\mathbf{h}}]$
(0, 0, 0)	0.084112	0	0.193796	0.010265	0.2881728	0.287635
(0.2, 0, 0)	0.3478324	0.090063	0.631211	0.01017	1.0792755	1.078947
(0.4, 0, 0)	1.1405797	0.36025	1.946794	0.012479	3.4601029	3.457646
(0.6, 0, 0)	2.4671303	0.810578	4.149386	0.011344	7.4384384	7.438045
(0.8, 0, 0)	4.33542	1.441003	7.255569	0.012427	13.04442	13.04394
(0, 0.4, 0)	0.0803783	0	0.186365	0.01014	0.2768827	0.276508
(0, 0, 2)	0.0831855	0	0.239748	0.003085	0.3260186	0.326543
(0.4, 0.4, 0)	1.1390122	0.360251	1.943502	0.010631	3.4533964	3.45301
(0.4, 0.4, 0.4)	0.9727806	0.304915	2.712194	0.009032	3.9989214	3.999269

In Fig. 6 we present curves obtained from the numerical values of $\widehat{W}_{\mathbf{x}_0}[\underline{\mathbf{h}}]$ and

$\overline{W}^{L}_{\mathbf{x}_0}[\underline{\mathbf{h}}]$ shown in Tab. 3 along the axis $(x_0, 0, 0)$. We can see that there is no visible difference between the two curves. Performing multiple regression with the software NLREG for the data of $\widehat{W}_{\mathbf{x}_0}[\underline{\mathbf{h}}]$ and x_0 from Tab. 3, we get the best regression for a biquadratic function, which has the form $\widehat{W}_{\mathbf{x}_0}[\underline{\mathbf{h}}] = 0.24020592\, {x_0}^4 + 19.7774191\, {x_0}^2 + 0.288290755$ and coefficient of determination $R^2 = 0.999999975$. In view of (68), (48) and (47), we can see from (83) that $\overline{W}^{L}_{\mathbf{x}_0}[\underline{\mathbf{h}}]$ is a quartic polynomial of x_0 $(\alpha_1\, {x_0}^4 + \alpha_2\, {x_0}^3 + \alpha_3\, {x_0}^2 + \alpha_4\, x_0 + \alpha_5)$ if $y_0 = z_0 = 0$. From the result of the regression and observation of some additional results of integration we conclude that the cofficients of x_0 and ${x_0}^3$ vanish, and the dependency between the two variables has biquadratic form.

Figure 6: Numerical values of $\widehat{W}_{\mathbf{x}_0}[\mathbf{h}]$ and $\overline{W}^{L}_{\mathbf{x}_0}[\mathbf{h}]$ for $y_0 = z_0 = 0$ and increasing values of x_0.

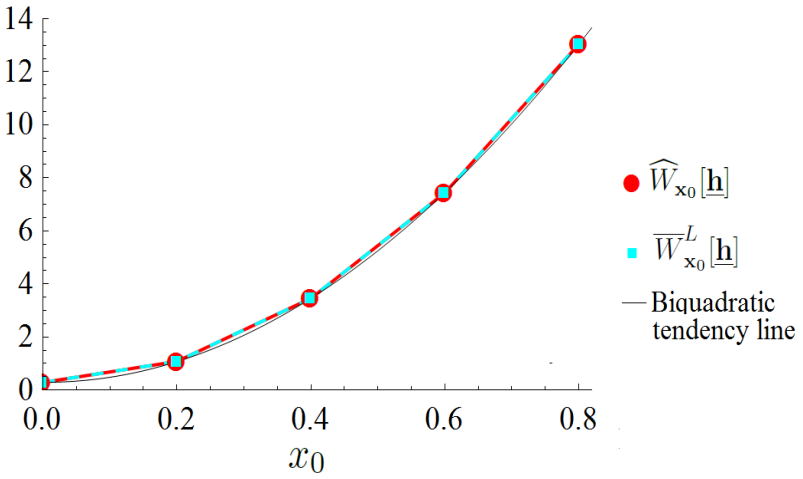

Source: Own author

4.4 Anti-plane shear experiment

The experiment of a circular shaft subjected to anti-plane shear is presented in Fig. 7. We consider no body forces and imposed displacements $\mathbf{u}(\rho = r_1) = \alpha\, \mathbf{e}_3$ and $\mathbf{u}(\rho = r_2) = \beta\, \mathbf{e}_3$. In classical linear elasticity, this surface traction yields the displacement field given by (HORGAN, 1995)

$$\mathbf{u} = u_3(\xi_1, \xi_2)\, \mathbf{e}_3, \tag{89}$$

and $u_3(\xi_1, \xi_2)$ must satisfy

$$\frac{\partial^2 u_3}{\partial {\xi_1}^2} + \frac{\partial^2 u_3}{\partial {\xi_2}^2} = 0, \qquad \text{in} \quad \mathcal{B}, \tag{90}$$

$$u_3 = \alpha, \quad \text{on} \quad \Omega_1 \quad \text{and} \quad u_3 = \beta, \quad \text{on} \quad \Omega_2, \tag{91}$$

where $\mathcal{B}$ is the circular hollow shaft and Ω_1 and Ω_2 represent its external and internal surface, respectively.

Figure 7: Shaft subjected to anti-plane shear.

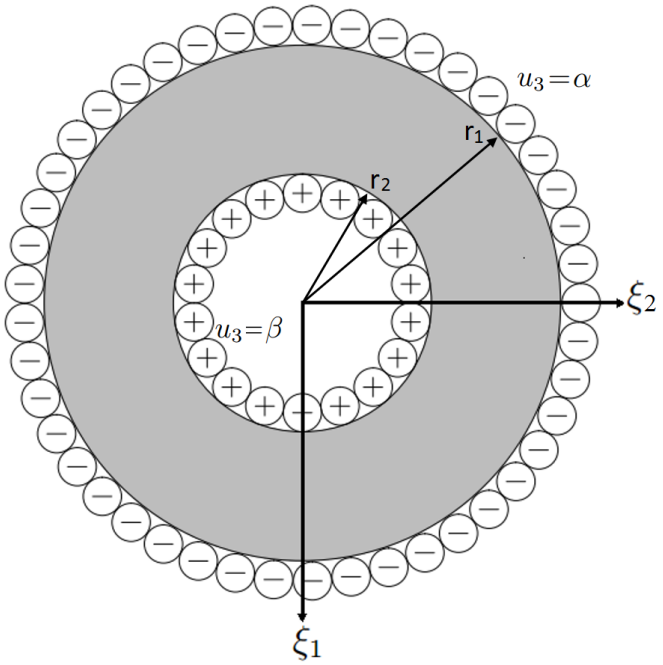

Source: Own author

Using polar coordinates (ρ, θ), parallel to the cross section of the shaft and centered at the origin $(\xi_1, \xi_2) = (0, 0)$, in (90) and considering axisymmetric deformation, we have

$$\frac{\partial^2 u_3}{\partial \rho^2} + \frac{1}{\rho}\frac{\partial u_3}{\partial \rho} = 0. \tag{92}$$

The solution of (92) is given by

$$u_3 = C_1 \, ln\, \rho + C_2. \tag{93}$$

Using the boundary conditions (91) in (93), the constants C_1 and C_2 are evaluated as

$$C_1 = \frac{\beta - \alpha}{ln\,(r_1/r_2)}, \qquad C_2 = \frac{ln\,({r_1}^{\alpha}/{r_2}^{\beta})}{ln\,(r_1/r_2)}. \tag{94}$$

Substituting $\rho = \sqrt{{\xi_1}^2 + {\xi_2}^2}$ and (94) into (93), we get

$$u_3(\xi_1, \xi_2) = \frac{\beta - \alpha}{ln\,(r_1/r_2)}\, ln\, \sqrt{{\xi_1}^2 + {\xi_2}^2} + \frac{ln\,({r_1}^{\alpha}/{r_2}^{\beta})}{ln\,(r_1/r_2)}. \tag{95}$$

Through (82), (89) and (95) we obtain the infinitesimal strain tensor $\mathbf{E}$ in the basis $\{\mathbf{e}_1, \mathbf{e}_2, \mathbf{e}_3\}$ as

$$[\mathbf{E}] = \frac{\beta - \alpha}{2({\xi_1}^2 + {\xi_2}^2)(ln\,(r_1/r_2))} \begin{bmatrix} 0 & 0 & \xi_1 \\ 0 & 0 & \xi_2 \\ \xi_1 & \xi_2 & 0 \end{bmatrix}.$$

To write the integrals of the free energy function, we repeat the procedure explained in Section 4.3. We get $\underline{\mathbf{h}}\langle\boldsymbol{\xi}\rangle$ considering the displacement field (95), and then use it to find $\underline{\varphi}\langle\boldsymbol{\xi}\rangle$ and $\underline{\mathbf{h}_d}\langle\boldsymbol{\xi}\rangle$. To calculate numerically the integrals, we consider the numerical values

$$\nu = 0.25,\ \delta = r_1/16, \tag{96}$$

for the mechanical properties and

$$r_1 = 8\,Ul,\ r_2 = r_1/2, \tag{97}$$

for the geometrical properties. Here too we consider that $\widetilde{\omega}(|\boldsymbol{\xi}|)$ is given by (86). The parameters α and β are removed from our calculations by dividing both sides of (47) by $(\beta - \alpha)^2$. So, from here on, in this section, we use the transformations $\widehat{W}_{\mathbf{x}_0}[\underline{\mathbf{h}}] = \widehat{W}_{\mathbf{x}_0}[\underline{\mathbf{h}}]/((\beta-\alpha)^2)$ and $\overline{W}^L_{\mathbf{x}_0}[\underline{\mathbf{h}}] = \overline{W}^L_{\mathbf{x}_0}[\underline{\mathbf{h}}]/(\beta-\alpha)^2$. The last term of (95), which contains α and β represent a rigid body translation and do not contribute to any other result presented.

The points chosen for the calculation of the free energy function and strain energy density function are distributed along four radial lines, as illustrated in Fig. 8. We consider five ponts on each line that are 4.5, 5, 6, 7 and 7.5 units of length far from the origin, and the angle between each line and the ξ_2-axis is equal to 0, 30, 45 and 90 degrees. Because the problem is axisymmetric, we can expect that the results are all the same for different lines. In fact, the results obtained for two points on different lines and at the same distance from the origin do not differ from each other. For this reason, we will show only the results for the points on one of the lines.

In Tab. 4, we present results of numerical integrations at five different points. The parameters A_{11}, A_{12}, A_{33} and A_{13} are the integrals defined in (87). Using the properties given in (96), the numerical values for the peridynamic constants are $\hat{\alpha}_{11} \approx 7.29513$, $\alpha_{12} \approx 7.29513$, $\alpha_{33} \approx 29.1805$ and $\hat{\alpha}_{13} \approx 554.83$. In Tab. 5 we present these values

Figure 8: Points considered for the anti-plane shear problem.

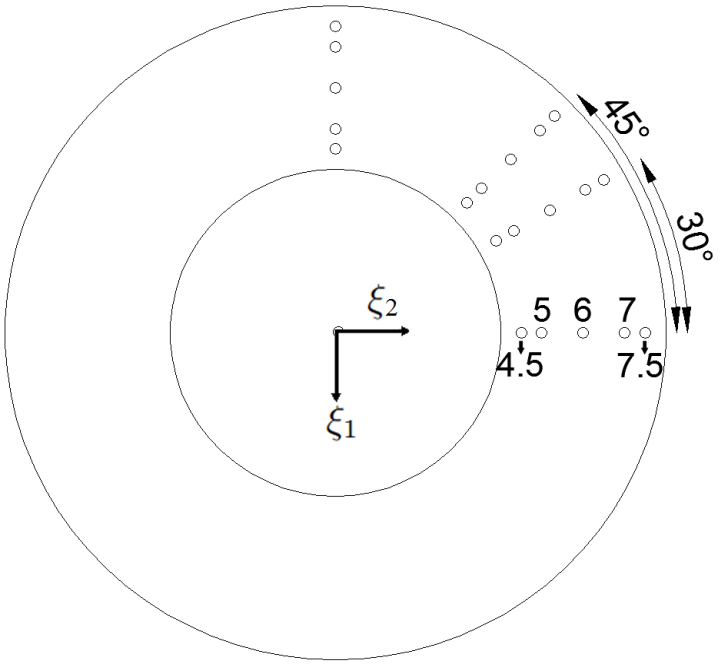

Source: Own author

multiplied by the values of Tab. 4. The last two columns of Tab. 5 contain values of the free energy function and the weighted average of the strain energy density. Comparing these two columns, we see that, also for the anti-plane shear problem, the correspondence argument (47) is approximately satisfied at the chosen points using the values given by (96) and (97). Using (88), the maximum percentage error between the values of the two columns is 0.017%, which is very small, in view of that the accuracy of the numerical integration is limited.

Table 4: Results of numerical integrations for the anti-plane shear problem

(x_0, y_0)	A_{11}	A_{12}	A_{33}	A_{13}
(0, 7.5)	0,00067655	0	0,000677064	$2,19175 \cdot 10^{-9}$
(0, 7)	0,00077669	0	0,000777359	$3,26743 \cdot 10^{-8}$
(0, 6)	0,00105733	0	0,0010586	$5,34805 \cdot 10^{-8}$
(0, 5)	0,00152296	0	0,00152559	$1,18999 \cdot 10^{-7}$
(0, 4.5)	0,00188057	0	0,00188449	$1,74136 \cdot 10^{-7}$

Fig. 9 presents the numerical values for $\widehat{W}_{\mathbf{x}_0}[\underline{\mathbf{h}}]$ and $\overline{W}^L_{\mathbf{x}_0}[\underline{\mathbf{h}}]$ along the axis $(0, y_0)$. We can see that there is no visible difference between the two graphs. Performing power regression with the software NLREG for the data of $\widehat{W}_{\mathbf{x}_0}[\underline{\mathbf{h}}]$ and y_0 from Tab. 5, we obtain

$\widehat{W}_{\mathbf{x}_0}[\underline{\mathbf{h}}] = 0.4221625\, {y_0}^{-2.0061641}$ and coefficient of determination $R^2 = 0.99999986$.

Table 5: Terms of free energy function and strain energy density for the anti-plane shear problem

(x_0, y_0)	$A_{11} \cdot \hat{\alpha}_{11}/2$	$A_{12} \cdot \alpha_{12}$	$A_{33} \cdot \alpha_{33}/4$	$A_{13} \cdot \hat{\alpha}_{13}/2$	$\widehat{W}_{\mathbf{x}_0}[\underline{\mathbf{h}}]$	$\overline{W}^L_{\mathbf{x}_0}[\underline{\mathbf{h}}]$
(0, 7.5)	0,002468	0	0,004939	$6,0803 \cdot 10^{-6}$	0,007413	0,007414
(0, 7)	0,002833	0	0,005671	$9,06435 \cdot 10^{-6}$	0,008513	0,008513
(0, 6)	0,003857	0	0,007723	$1,48363 \cdot 10^{-5}$	0,011594	0,011595
(0, 5)	0,005555	0	0,011129	$3,30121 \cdot 10^{-5}$	0,016718	0,016718
(0, 4.5)	0,00686	0	0,013748	$4,83078 \cdot 10^{-5}$	0,020655	0,020659

Figure 9: Numerical values of $\widehat{W}_{\mathbf{x}_0}[\mathbf{h}]$ and $\overline{W}^L_{\mathbf{x}_0}[\mathbf{h}]$ plotted for points on the ξ_2-axis in Fig. (8).

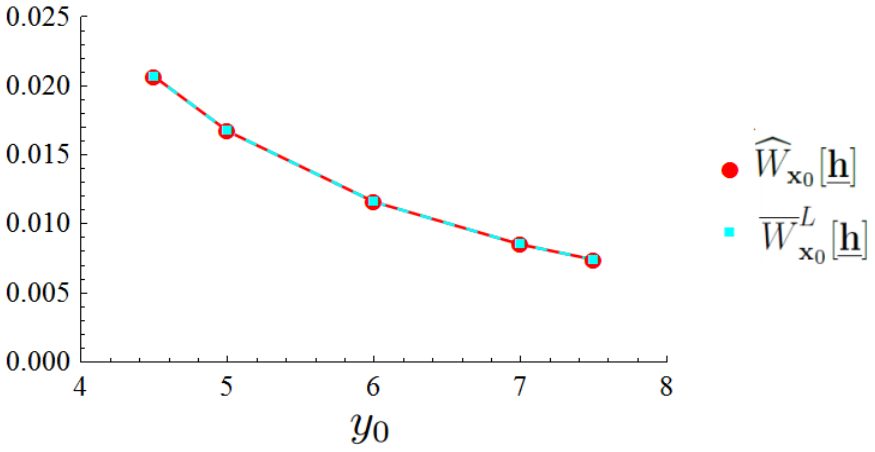

Source: Own author

5 PERIDYNAMIC BAR

In this section, we consider linear elastic peridynamic bars of finite length being pulled at the ends and having micromoduli introduced by authors cited in Section 2.2. We formulate the problem of a cylindrical bar in equilibrium without body force being subjected to imposed displacements at its ends. Then we present the numerical scheme used to obtain approximate solutions for the problem. We concentrate our attention on a particular micromodulus that yields a singular behavior of the solution near the ends and study both convergence of the proposed numerical scheme and convergence of the nonlocal model to the classical linear elastic model as the horizon δ tends to zero.

5.1 1-D peridynamic model

To arrive at a one-dimensional peridynamic theory for a cylindrical bar of finite length and constant cross-sectional area A, we start by assuming that the generators of the bar are parallel to the x-axis. We then integrate the vector equation (9) over the cross section $\mathcal{A}$ at an arbitrary coordinate ξ_1 and divide the resulting expression through by A. We further assume that the only non-zero equation that results from the above consideration is given by

$$\rho\ddot{u}(x) = \int_{-\delta}^{L+\delta} f(x,\, \hat{x})d\hat{x} + b(x),$$

where

$$u(x) = \frac{1}{A}\int_{\mathcal{A}} u_1(\mathbf{x})dA, \qquad b(x) = \frac{1}{A}\int_{\mathcal{A}} b_1(\mathbf{x})dA,$$

and

$$f(x,\, \hat{x}) = \frac{1}{A}\int_{\mathcal{A}}\int_{\mathcal{N}} f_1(\mathbf{x},\, \hat{\mathbf{x}})dA'dA, \tag{98}$$

in which u_1, b_1 and f_1 are the longitudinal components of $\mathbf{u}$, $\mathbf{b}$ and $\mathbf{f}$, respectively, and $dv_\xi = dA\,dx$ has been used.

The scalar force between particles, given by f in (98) is related to their relative displacements through the constitutive relation

$$f(x,\, \hat{x}) = \hat{f}(u(\hat{x}) - u(x),\, \hat{x} - x), \tag{99}$$

where the constitutive response function $\hat{f}$ satisfies

$$\hat{f}(\eta, \xi) = -\hat{f}(-\eta, -\xi), \quad \forall\, \eta, \xi,$$

so that Newton's third law is identically satisfied.

In this work we consider linear elastic peridynamic materials, so that

$$\hat{f}(\eta, \xi) = C(\xi)\eta, \tag{100}$$

where C is the micromodulus of the material and is analogous to the Young's modulus of classical linear elasticity. In the next two sections we present different expressions of C in terms of E that are found in the literature.

To satisfy (99), we require that $C(\xi) = C(-\xi)$. In addiction we consider that $C(\xi) = 0$ for $|\xi| > \delta$, where δ is the horizon.

5.2 Finite bar pulled at the ends

Let $[0, L]$ be the interval occupied by an one-dimensional bar in its natural state. The bar is made of the linear peridynamic material given by (100). Because of the nonlocal behavior of the bar, we extend the interval of definition of the axial displacement u to $[-\delta, L+\delta]$, in such a way that boundary conditions are prescribed on the intervals $[-\delta, 0]$ and $[L, L+\delta]$.

The equilibrium equation without body force at a point $x \in (0, L)$ of the peridynamic bar may be written as

$$\int_{-\delta}^{L+\delta} C(x' - x)[u(x') - u(x)]\mathrm{d}x' = 0\,, \quad \forall x \in [0, L]\,. \tag{101}$$

On the extended parts of the bar, we impose displacement boundary conditions, so that

$$u(x') = \bar{u}(x') \text{ for } x' \in [-\delta, 0] \bigcup [L, L+\delta]\,. \tag{102}$$

We then have that the problem of equilibrium without body force of the peridynamic bar consists of finding the axial displacement $u : (0, L) \to \mathbb{R}$ that satisfies the governing equation (101) together with the boundary conditions given by (102). In Fig. 10 we

ilustrate the bar being pulled by a constant displacement Δ. In this case, $\bar{u}(x') = 0$ for $x' \in [-\delta, 0]$ and $\bar{u}(x') = \Delta$ for $x' \in [L, L+\delta]$.

Figure 10: Finite bar of length L pulled at the ends with imposed displacement Δ.

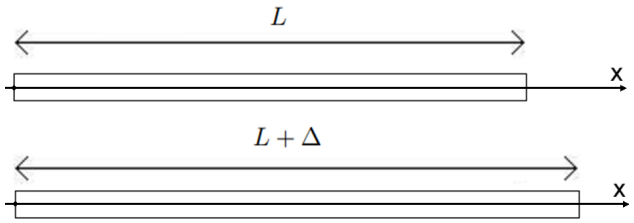

Source: Own author

Now, let

$$C_0 = \int_{-\delta}^{\delta} C(\xi)\mathrm{d}\xi \tag{103}$$

and observe from (101) that

$$0 = \int_{-\delta}^{L+\delta} C(x'-x)u(x')\mathrm{d}x' - C_0\, u(x) = \int_{0}^{L} C(x'-x)u(x')\mathrm{d}x' - C_0\, u(x) + \int_{-\delta}^{0} C(x'-x)\bar{u}(x')\mathrm{d}x' + \int_{L}^{L+\delta} C(x'-x)\bar{u}(x')\mathrm{d}x'\,.$$

This can be rewritten in the form

$$u(x) - \frac{1}{C_0}\int_{0}^{L} C(x'-x)u(x')\mathrm{d}x' = \frac{g(x)}{C_0}\,, \qquad \forall\, x \in (0, L)\,, \tag{104}$$

where

$$g(x) = \int_{-\delta}^{0} C(x'-x)\bar{u}(x')\mathrm{d}x' + \int_{L}^{L+\delta} C(x'-x)\bar{u}(x')\mathrm{d}x'\,. \tag{105}$$

The integral equation (104) together with (105) yield an inhomogeneous Fredholm equation of the second kind, where the role of the kernel is played by the micromodulus function and the function $g(x)$ depends only on the boundary data. Conditions for existence of solutions are associated with the form of the kernel (PORTER; STIRLING,

1990). Granted that a solution exists, the equation can be easily solved numerically. Recall from a comment in Section 2.2 that a Fourier transform technique is used to find a closed form solution for the case of infinite domains.

In the case of constant micromodulus function, given by

$$C(\xi) = \begin{cases} 3\,E/\delta^3 & \text{if } \ |\xi| \leq \delta\,, \\ \\ 0 & \text{if } \ |\xi| > \delta\,, \end{cases} \tag{106}$$

where E is the Young's modulus, and assuming that the boundary conditions are given by

$$\bar{u}(x) = \begin{cases} 0 & \text{if } \ x \in (-\delta, 0)\,, \\ \\ \Delta & \text{if } \ x \in (L, L+\delta)\,, \end{cases} \tag{107}$$

one finds from (103) that $C_0 = 6E/\delta^2$ and from (105) that

$$g(x) = \begin{cases} 0 & \text{if } 0 \leq x < L-\delta\,, \\ \\ 3\frac{E\,\Delta}{\delta^3}(x - L + \delta) & \text{if } L-\delta \leq x \leq L\,. \end{cases}$$

5.3 Numerical results and Discussion

We show numerical results for the four expressions of micromoduli presented below.

$$C(\xi) = \begin{cases} 3E/\delta^3 & \text{(constant micromodulus)}, \\ \\ [4\,E/(\delta^3\,\sqrt{\pi})]\,e^{-(\xi/\delta)^2} & \text{(exponencial micromodulus)}, \\ \\ (12\,E/\delta^3)(1 - |\xi|/\delta) & \text{(triangular micromodulus)}, \\ \\ (6\,E/\delta^2)(1 - |\xi|/\delta)/|\xi| & \text{(singular micromodulus)}. \end{cases} \tag{108}$$

In all cases, the micromoduli are proportional to E in the interval $(-\delta, \delta)$ and zero elsewhere. It follows from either (101) or (104) together with both (103) and (105) that the numerical results do not depend on the value of E and, therefore, this value will be ignored in the following computations. Also, the expression for the constant micromodulus is the same one given by (106). The references where, to the best of our knowledge, the corresponding expression first appeared are Silling, Zimmermann e Abeyaratne (2003) for constant micromodulus, Weckner, Brunk e Epton (2009) for exponencial micromodulus,

and Bobaru et al. (2009) for the singular micromodulus. The triangular micromodulus is introduced in this work.

The graphs of the micromoduli given by (108) are presented in Fig. 11. Notice that the three limited micromoduli are normalized to have $C(0) = 1$ and for all of them $C(\xi) = 0 \quad \text{if} \quad |\xi| > \delta$. We can see from the figure that the triangular micromodulus is continuous and piecewise linear, both constant and exponencial micromoduli are smooth at the origin, and discontinuous at $\pm\delta$, and the singular micromodulus is continuous, except at the origin.

Figure 11: Shape of the micromodulus functions, $C(\xi)$, for $|\xi| \leq \delta$.

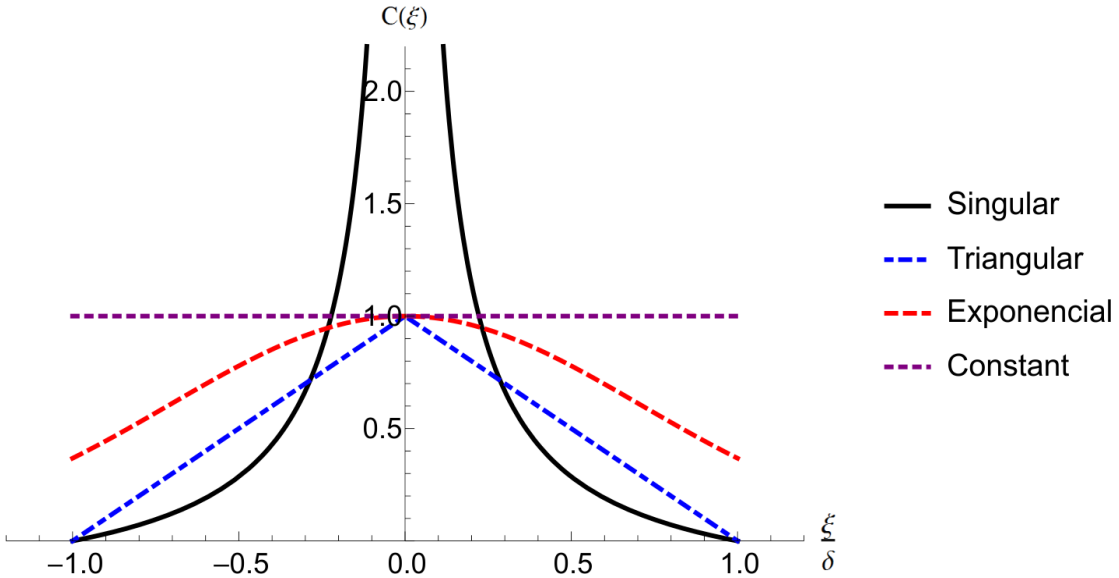

Source: Own author

The particularly simple form of the expression (101) allows a straightforward implementation of a numerical scheme, which can be extended to higher dimensions, for the numerical calculation of the displacement field of the peridynamic bar. An alternative numerical scheme[1], based on the Fredholm equation (104) together with both (103) and (105), has also been implemented, but will not be presented here. Considering the boundary conditions (107), we first introduce the new variables $x \to x\,L$ and $u \to u/\Delta$, where, now, $x \in (0, 1)$ and $u(x) \in (0, 1)$, into (101) and rewrite this expression as

$$\int_{-\delta}^{1+\delta} C((x' - x)\,L)[u(x') - u(x)]\mathrm{d}x' = 0\,, \quad \forall x \in [0, 1]\,. \tag{109}$$

[1]The scheme is based on a computational code available at <http://mathematica.stackexchange.com/questions/104667/solving-fredholm-equation-of-the-2nd-kind>, which is written in the program Mathematica®.

where we have introduced the definition $\delta \to \delta\, L$.

In the simplest approach, one can divide the interval $(-\delta, 1+\delta)$ into $N+1+2n$ equidistant nodes such that $x_{-n} = -\delta$, $x_0 = 0$, $x_N = 1$ and $x_{N+n} = 1+\delta$. We then have that the distance between nodes is constant and given by $h = 1/N = \delta/n$ and that the discretized form of the equilibrium equation (109) becomes the system of $N+1$ equations

$$\sum_{j=-n}^{N+n} C((x_i - x_j)\, L)[u(x_i) - u(x_j)]h = 0\,, \qquad i = 0, ..., N\,. \tag{110}$$

In Fig. 12 we illustrate the discretized bar and the boundary conditions. In this work we consider geometric sequences of nodes starting with both $N = 1000$ and $n = 20$ and having a factor of 2. Substituting $C(\xi)$, given by one of the expressions in (108), into the system of equations (110), we can solve for $u(x_i)$, $i = 0, \ldots, N$, and obtain an approximate expression for the displacement field $u(x)$.

Figure 12: Representation of the discretized bar and boundary conditions.

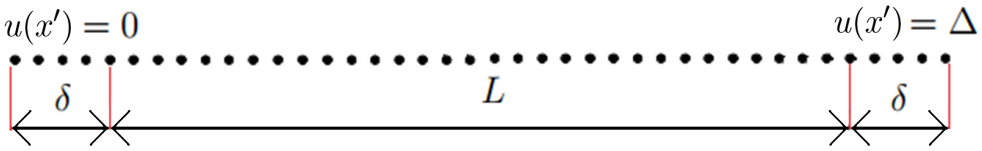

Source: Own author

To investigate the influence of the horizon δ on the solution of the integral equation (101), we consider the constant micromodulus given by either (106) or the first expression in (108) and the four horizons $\delta = 1/2,\ 1/5,\ 1/10,\ 1/50$. In Fig. 13 we show the displacement $u(x)$ plotted against the position $x \in (0, 1)$ for these four horizons and $N = 16000$ nodes, which corresponds to the most refined mesh in this work. We see from this figure that (i) the end points of the graphs tend to the points $(0, 0)$ on the left end and $(1, 1)$ on the right end of the bar as δ decreases; (ii) the solution is highly nonlinear in boundary layers of length δ near the ends and almost linear outside these boundary layers. In fact, the sequence of solutions tends to the solution of the corresponding problem in the classical linear elasticity theory as $\delta \to 0$, which is linear and satisfies the boundary conditions exactly. This classical solution is represented by the thin solid line in the figure.

Thus, we see from these observations that displacement discontinuities appear at the ends of the bar for a fixed $\delta > 0$. The jumps are finite and decrease as the horizon decreases. Displacement discontinuities have already been observed for infinite peridyna-

Figure 13: Displacement $u(x)$ versus position $x \in (0,1)$ obtained from classical linear elasticity and from peridynamics for the constant micromodulus, $N = 16000$, and four values of the horizon δ.

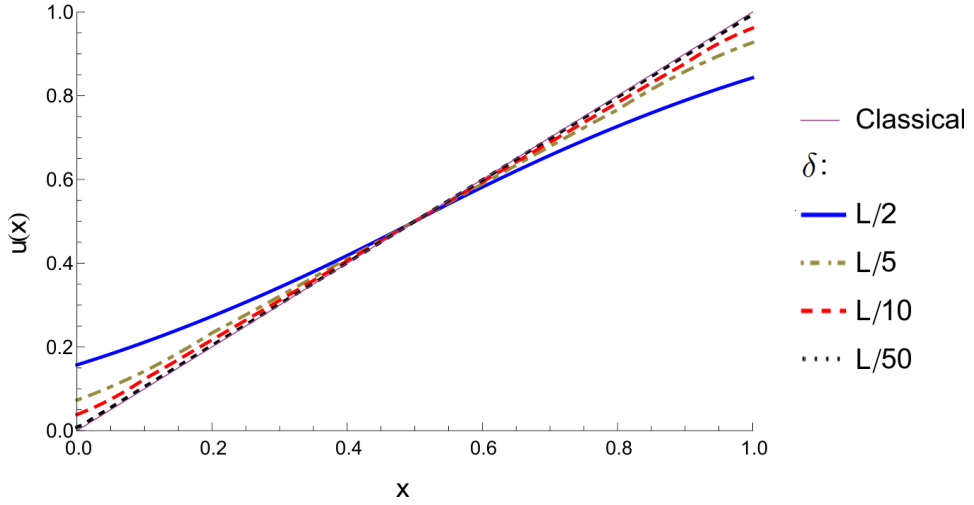

Source: Own author

mic bars under concentrated loads (SILLING; ZIMMERMANN; ABEYARATNE, 2003; WECKNER; ABEYARATNE, 2005; MIKATA, 2012), but have not been reported yet for finite bars subjected to displacement conditions at the ends.

The reason for the formation of the discontinuities is clear from the analysis of the field equation (109), which expresses, for each particle $x \in (0,1)$ and the corresponding set of particles in its δ-neighborhoood, the equilibrium of the forces exerted by the particles on the left- and right-hand sides of x. Thus, for a particle at $x = 0$, the particles on the interval $(-\delta, 0)$ cannot move and the resultant of the forces on the left hand side must be in equilibrium with the forces on the right-hand side, producing a strain localization. Then, as $x \to 0^+$, we have from the left-hand side that

$$\int_{-\delta}^{0} C((x'-x)\,L)[u(x')-u(x)]\mathrm{d}x' = -[3\,E/(\delta\,L)^3]\,u(x)\,\delta$$

and from the right-hand side that

$$\int_{0}^{\delta} C(x'-x)[u(x')-u(x)]\mathrm{d}x' = [3\,E/(\delta\,L)^3]\,(\int_{0}^{\delta} u(x')\mathrm{d}x' - u(x)\,\delta).$$

We then have that $u(0^+) = \int_0^\delta u(x')\mathrm{d}x'/(2\,\delta)$, that is, as we approach the origin from the right-hand side, the value of $u(x)$ is half of the average of the displacement field evaluated on the right-hand side of the origin. An analogous argument holds for $x \to 1$.

We now show that the field equation (109) converges to the second order ordinary

differential equation of classical linear elasticity as $\delta \to 0$ for the case of the constant micromodulus. Such demonstration is usually done by using linear displacements as test functions (SILLING; ZIMMERMANN; ABEYARATNE, 2003; MIKATA, 2012). Here, however, it is done directly. For $x \in (0,1)$, straightforward applications of the l'Hôpital rule yield

$$
\begin{aligned}
0 &= L^3 \lim_{\delta\to 0} \int_{-\delta}^{1+\delta} C((x'-x)\,L)[u(x')-u(x)]\mathrm{d}x' = \lim_{\delta\to 0} \frac{3E}{\delta^3}\Big(\int_{x-\delta}^{x+\delta} u(x')\mathrm{d}x' - 2\delta u(x)\Big) \\
&= \lim_{\delta\to 0} \frac{E}{\delta^2}\Big([u(x+\delta)-u(x-\delta)] - 2u(x)\Big) = \lim_{\delta\to 0} \frac{E}{2\delta}[u'(x+\delta)-u'(x-\delta)] \\
&= \lim_{\delta\to 0} \frac{E}{2}[u''(x+\delta)+u''(x-\delta)] = Eu''(x)\,.
\end{aligned}
$$

Next, we consider the four micromoduli given by (108), the horizon $\delta = 1/50$ and $N = 16000$ nodes, which corresponds to the most refined mesh in this work. Because of the relation $1/N = \delta/n$ introduced above, we have that $n = 320$ nodes. We then show in Fig. 14 the displacement $u(x)$ plotted against the reference position $x \in (0, 0.006)$. For comparison purposes, we also show a graph for the displacement $u(x)$ obtained from the exact solution of the bar problem in the context of the classical linear elasticity theory. Observe from this figure that all the curves obtained from peridynamics are above the curve obtained from the classical theory, are almost parallel to each other away from the origin, and tend to different values as we approach the origin from its right-hand side. Following arguments that are similar to those presented above in the analysis of the constant micromodulus case, we have verified that these values are approximations of the expression

$$
u(0^+) = \int_0^{\delta} C((x'-x)\,L)\,u(x')\mathrm{d}x' \Big/ \left(2\int_0^{\delta} C((x'-x)\,L)\,\mathrm{d}x'\right)\,.
$$

In the case of the singular micromodulus, we can rewrite this expression in the form

$$
u(0^+) = \int_0^{\delta} C((x'-x)\,L)\,[u(x')-u(0^+)]\mathrm{d}x' \Big/ \int_0^{\delta} C((x'-x)\,L)\,\mathrm{d}x'\,,
$$

and, provided that $u(0^+)$ is finite, observe that the integrand in the numerator is less singular than the integrand in the denominator, which tends to infinity as $x \to 0^+$. Thus,

Figure 14: Displacement $u(x)$ versus position $x \in (0, 0.006)$ obtained from classical linear elasticity and from peridynamics for $\delta = 1/50$, $N = 16000$, and four different micromoduli C.

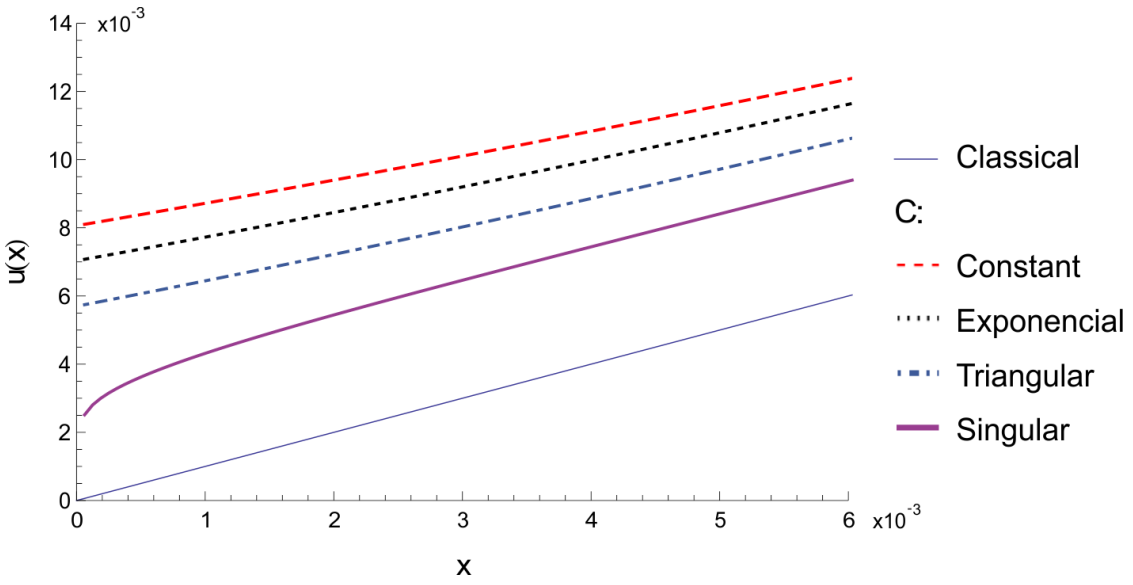

Source: Own author

we have that $u(x) \to 0$ as $x \to 0^+$.

To see the difference on the behavior of the solution for different micromoduli near the ends, we have considered a node at $x > 0$ and its immediate neighbor on its right-hand side and evaluated the relative position Δx between the two nodes as well as their relative displacement $\Delta u(x)$ using peridynamics for the fixed values $\delta = 1/50$ and $N = 16000$ and the four micromoduli shown in Fig. 14. We have then obtained Fig. 15 showing graphs of the ratio $\Delta u(x)/\Delta x$ versus $x \in (0, 0.002)$ for the different micromoduli. We see from the figure that three of the curves are very similar, corresponding to ratios that are almost constant and tend to a finite value as x tends to zero. For the singular micromodulus the ratio $\Delta u(x)/\Delta x$ seems to become unbounded as x tends to zero.

From now on, we consider the singular micromodulus only, which is given by the last expression in (108). To investigate convergence of the numerical scheme, we show in Fig. 16 the displacement $u(x)$ plotted against the reference position $x \in (0, 0.003)$ for increasing numbers of nodes and for the horizon $\delta = 1/50$. Again, for comparison purposes, we also show the graph of $u(x)$ versus x obtained from the exact solution of the bar problem in the context of the classical linear elasticity theory. We see from this figure that all the curves obtained from peridynamics are nearly parallel to the curve obtained from the classical linear theory away from the origin, the displacement fields obtained from peridynamics converge to a limit field as the number of nodes increases

Figure 15: Ratio between relative displacement $\Delta u(x)$ and relative position Δx versus position $x \in (0, 0.002)$ obtained from peridynamics for $\delta = 1/50$, $N = 16000$, and four different micromoduli.

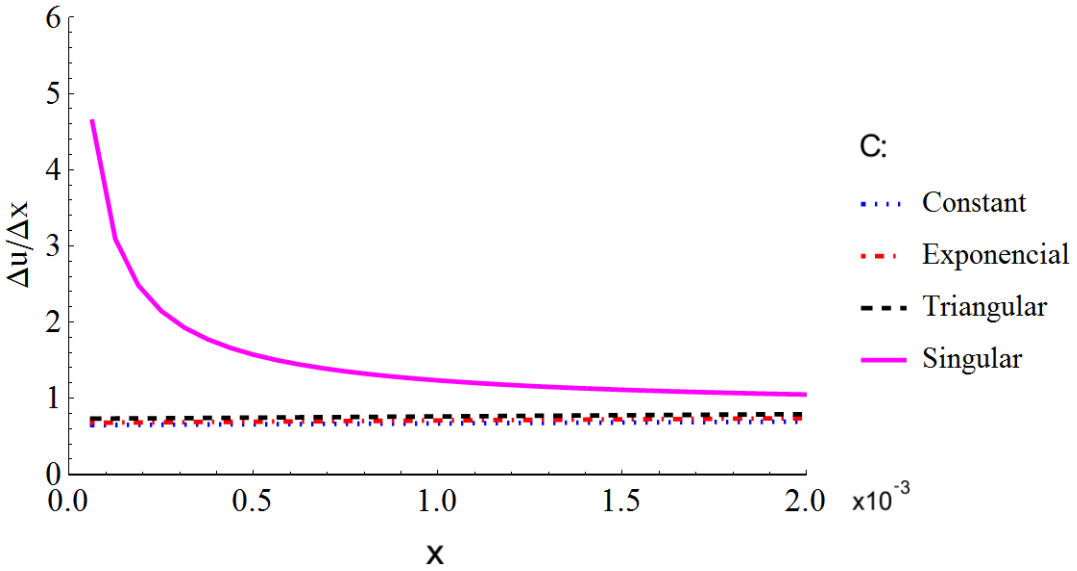

Source: Own author

geometrically, and this limit field seems to have unbounded derivative at $x = 0$.

Figure 16: Displacement $u(x)$ versus position $x \in (0, 0.003)$ obtained from classical linear elasticity and from peridynamics for the singular micromodulus, $\delta = 1/50$, and an increasing number of nodes N.

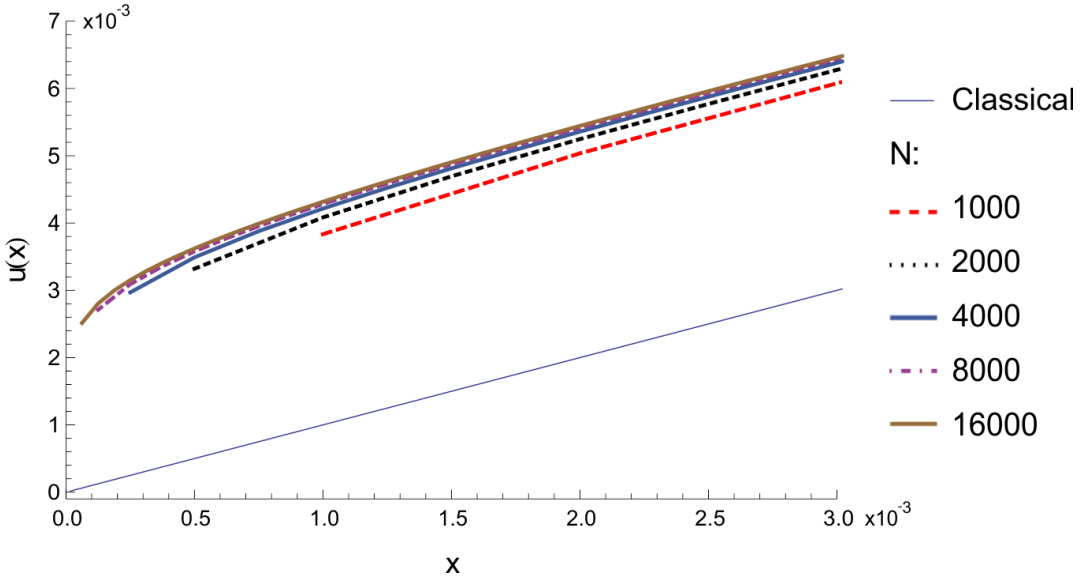

Source: Own author

To see the last feature above more clearly, we have evaluated a more detailed version of the ratio between $\Delta u(x)$ and Δx corresponding to the singular micromodulus in Fig. 15, in which we can see the convergence of the numerical scheme, using the values of N shown in Fig. 16. We have then obtained Fig. 17 showing graphs of the ratio

$\Delta u(x)/\Delta x$ versus $x \in (0, 0.003)$ for the fixed value $\delta = 1/50$ and increasing values of N. A diamond symbol on a curve yields the position of the first node to the right of the origin corresponding to a discretization with the number of nodes shown next to the symbol. We then see from the figure that all the curves are on the top of each other for $x \geq 0.001$, which corresponds to the position of the first node in a discretization with 1000 nodes. We also see that the ratio $\Delta u(x)/\Delta x$ becomes unbounded as the mesh becomes refined, with the curves corresponding to less refined meshes being indistinguishable from the curve corresponding to a more refined mesh.

Figure 17: Ratio between relative displacement $\Delta u(x)$ and relative position Δx versus position $x \in (0, 0.003)$ obtained for the singular micromodulus, $\delta = 1/50$, and increasing number of nodes N.

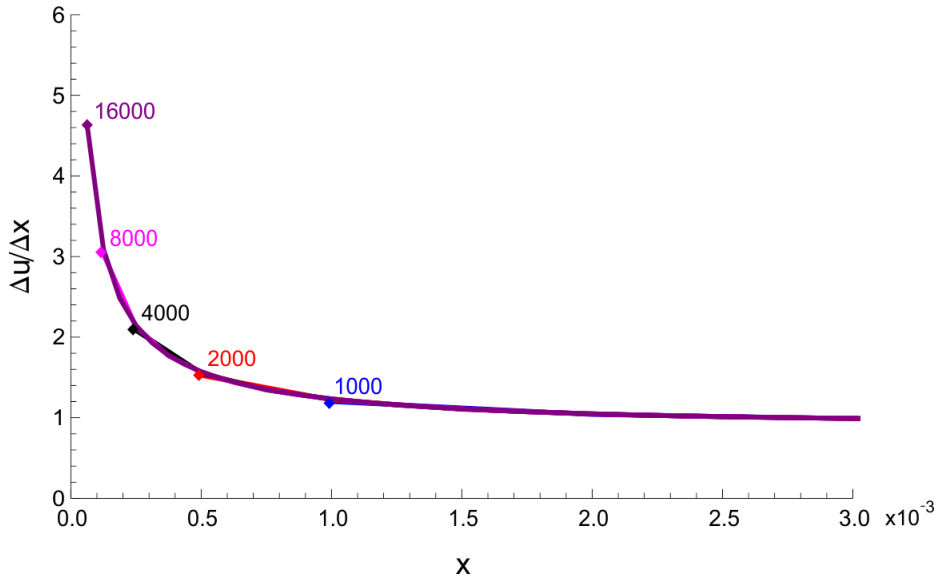

Source: Own author

In Fig. 18 we hold $N = 16000$ fixed and show the displacement $u(x)$ plotted against the reference position $x \in (0, 1)$ for decreasing values of the horizon δ. Again, for comparison purposes, we also show the graph of $u(x)$ versus x obtained from the classical linear elasticity theory. Observe from this figure that the peridynamic solutions tend to the classical solution as δ decreases. To investigate the behavior of these curves near the origin, we have plotted Fig. 19, which shows $u(x)$ against x in the interval $(0, 0.006)$. Observe from this figure that $u(x)$ obtained from peridynamics is highly nonlinear near the origin, tends to $u(x)$ obtained from classical theory as $\delta \to 0$, and, as observed earlier, seems to have unbounded derivative at $x = 0$.

Figure 18: Displacement $u(x)$ versus position $x \in (0, 1)$ obtained from classical linear elasticity and from peridynamics using $N = 16000$ and decreasing values of the horizon δ.

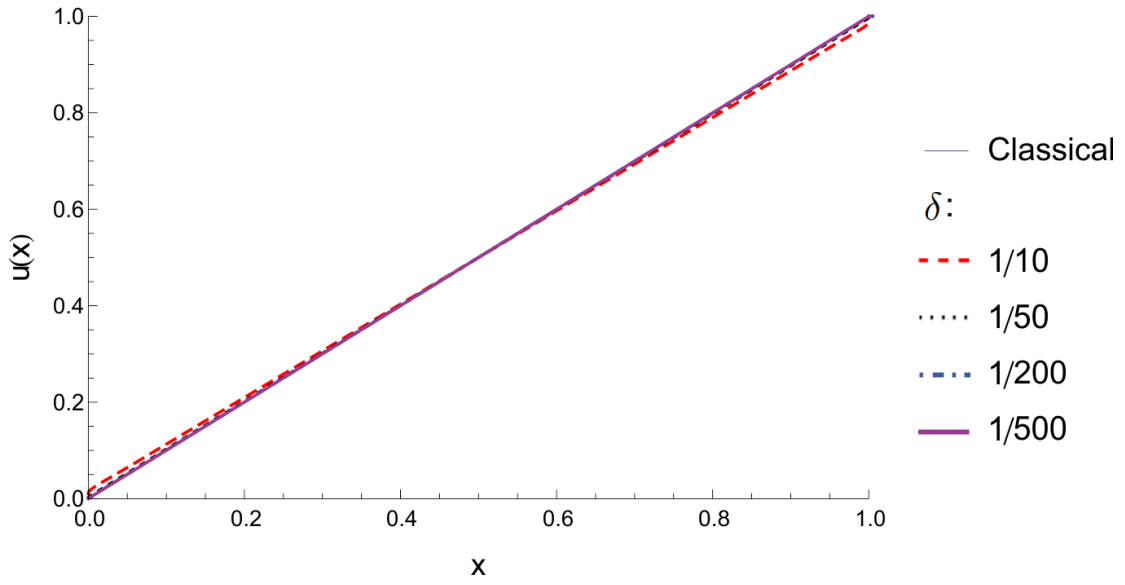

Source: Own author

Figure 19: Displacement $u(x)$ versus position $x \in (0, 0.006)$ obtained from classical linear elasticity and from peridynamics using $N = 16000$ and decreasing values of the horizon δ.

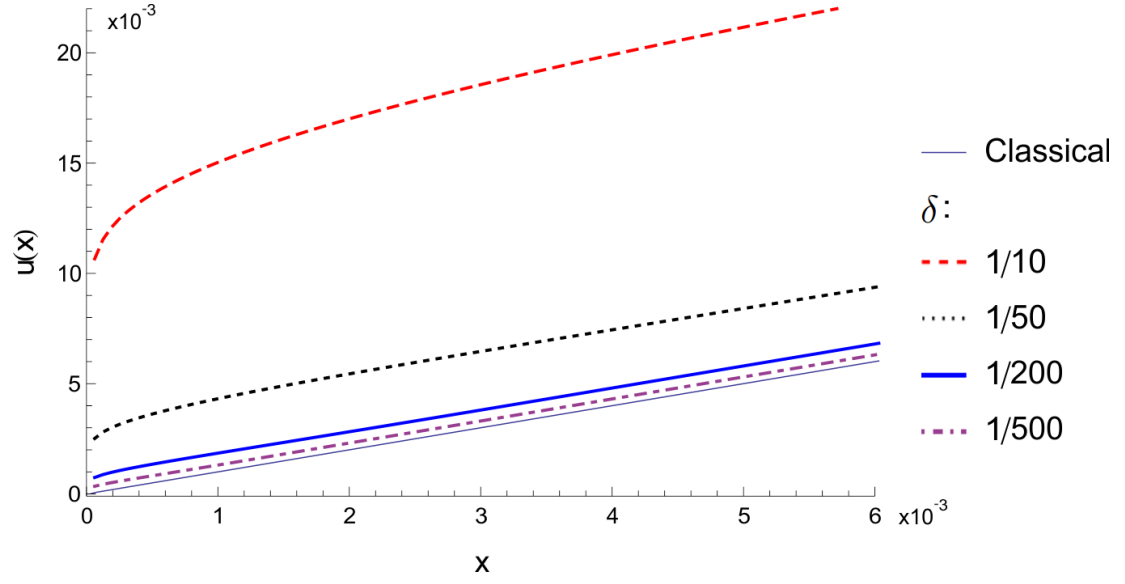

Source: Own author

6 CONCLUSIONS

Three of the four peridynamic constants that appear in the free energy function defined by (18) were previously determined in Aguiar e Fosdick (2014) and Aguiar (2016). From (39) it is noted that, to determine the fourth constant $\hat{\alpha}_{13}$, we need to consider a deformation state in which both $\mathbf{h}_d$ and $\underline{\varphi}$ do not vanish. Considering the pure bending experiment and using the correspondence argument between the free energy function and the weighted average of the strain energy density function from classical elasticity theory, in the form of (47), we obtain a relation between $\hat{\alpha}_{13}$ and the elastic constants from classical theory, which is given by (67).

We have verified the validity of the closed form expressions for the peridynamic constants by using displacement fields from classical linear elasticity for both beam bent by terminal loads and circular shaft subjected to anti-plane shear experiments. We set numerical values for the material and geometrical properties and use the expressions for the peridynamic constants to numerically calculate the free energy function and the weighted average of the strain energy density function at selected points in the domain. The results shown in Tab. 3, Tab. 5, Fig. 6 and Fig. 9 show that the correspondence argument is nearly satisfied for the above experiments.

We have also investigated the one-dimensional problem of a linear elastic peridynamic bar of length L being pulled at the ends by imposed displacements on extended parts of the bar having length δ. We have shown that the problem can be formulated in terms of an inhomogeneous Fredholm equation of the second kind, which assumes a simple form in the case of a constant micromodulus. We have then used a numerical scheme to obtain approximate solutions for the peridynamic problem using different expressions of micromodulus, horizons, and discretizations. Except for the singular micromodulus, all the other micromoduli yield discontinuous displacements at the ends of the bar. Discontinuous displacements have been reported in the study of infinity bars, but not of finite bars. The singular micromodulus gives continuous displacements, but unbounded derivatives of displacements, at these ends. We have then focused our attention in the investigation of this singular case and found that the approximate solutions of the peridynamic problem converge to the classical solution of linear elasticity for vanishing horizon and a fixed discretization. Also, for a fixed horizon, these solutions converge to a limit function as the mesh is refined. The information obtained from the investigation of the one-dimensional

peridynamic problem can now be applied to better understand the behavior of solutions in higher dimensions and to design effective numerical schemes for higher-dimensional problems.

REFERENCES

AGUIAR, A. On the determination of a peridynamic constant in a linear constitutive model. *Journal of Elasticity*, v. 122, p. 27–39, 2016.

AGUIAR, A.; FOSDICK, R. A constitutive model for a linearly elastic peridynamic body. *Mathematics and Mechanics of Solids*, v. 19, n. 5, p. 502–523, 2014.

AGUIAR, A. R. *Uma contribuição ao desenvolvimento da teoria peridinâmica*. 2015. 100 p. Free teaching Thesis - Department of Structural Engineering, São Carlos School of Engineering, University of São Paulo, São Paulo. 2015.

ASKARI, E.; XU, J.; SILLING, S. Peridynamic analysis of damage and failure in composites. In: *44th AIAA Aerospace Sciences Meeting and Exhibit*. 2006.

BOBARU, F. et al. Convergence, adaptive refinement, and scaling in 1d peridynamics. *International Journal for Numerical Methods in Engineering*, v. 77, n. 6, p. 852–877, 2009.

DAYAL, K.; BHATTACHARYA, K. Kinetics of phase transformations in the peridynamic formulation of continuum mechanics. *Journal of the Mechanics and Physics of Solids*, v. 54, n. 9, p. 1811–1842, 2006.

DIYAROGLU, C. et al. Peridynamic modeling of composite laminates under explosive loading. *Composite Structures*, v. 144, p. 14–23, 2016.

ERINGEN, A. C.; EDELEN, D. G. B. On nonlocal elasticity. *International Journal of Engineering Science*, v. 10, n. 3, p. 233–248, 1972.

ERINGEN, A. C.; KIM, B. S. Stress concentration at the tip of crack. *Mechanics Research Communications*, v. 1, n. 4, p. 233–237, 1974.

GERSTLE, W.; SAU, N.; SILLING, S. A. Peridynamic modeling of plain and reinforced concrete structures. In: International Conference on Structural Mechanics in Reactor Technology, 18. *Proceedings. . .* , Beijing, China. 2005.

GLAWS, A. T. *Finite element simulations of two dimensional peridynamic models*. 2014. 36 p. Dissertation (M. Sc. in Mathematics) - Faculty of the Virginia Polytechnic Institute and State University, Virgínia, EUA. 2014.

GRIFFITH, A. A. The phenomena of rupture and flow in solids. *Philosophical Transactions of the Royal Society of London A*, v. 221, n. 582-593, p. 163–198, 1921.

HA, Y. D.; LEE, J.; HONG, J. Fracturing patterns of rock-like materials in compression captured with peridynamics. *Engineering Fracture Mechanics*, v. 144, p. 176–193, 2015.

HORGAN, C. Anti-plane shear deformations in linear and nonlinear solid mechanics. *Society for Industrial and Applied Mathematics Review*, v. 37, n. 1, p. 52–81, 1995.

HU, W.; HA, Y. D.; BOBARU, F. Peridynamic model for dynamic fracture in unidirectional fiber-reinforced composites. *Computer Methods in Applied Mechanics and Engineering*, v. 217-220, p. 247–261, 2012.

HU, W. et al. Impact damage on a thin glass plate with a thin polycarbonate backing. *International Journal of Impact Engineering*, v. 62, p. 152–165, 2013.

KRONER, E. Elasticity theory of materials with long range cohesive forces. *Journal of Solids and Structures*, v. 3, n. 5, p. 731–742, 1967.

KUNIN, A. *Elastic Media with Microstructure I: One-Dimensional Models*. Berlin: Springer, 1982.

LEHOUCQ, R.; SILLING, S. Force flux and the peridynamic stress tensor. *Journal of the Mechanics and Physics of Solids*, v. 56, n. 4, p. 1566–1577, 2008.

LITTLEWOOD, D. J.; MISH, K.; PIERSON, K. Peridynamic simulation of damage evolution for structural health monitoring. *Mechanics of Solids, Structures and Fluids*, v. 8, p. 1–8, 2012.

MADENCI, E.; OTERKUS, E. *Peridynamic theory and its applications*. New York: Springer, 2014.

MIKATA, Y. Analytical solutions of peristatic and peridynamic problems for a 1d infinite rod. *International Journal of Solids and Structures*, v. 49, n. 21, p. 2887–2897, 2012.

OTERKUS, E. *Peridynamic theory for modeling three-dimensional damage growth in metallic and composite structures*. 2010. 208 p. Thesis (PhD in Aerospace Engineering) - Department of Aerospace and Mechanical Engineering, University of Arizona, Tucson, EUA. 2010.

OTERKUS, E.; BARUT, A.; MADENCI, E. Damage growth prediction from loaded composite fastener holes by using peridynamic theory. In: *Structures, Structural Dynamics and Materials Conference*, 51, Orlando, Florida. Collection of technical papers, Orlando: AAIA. 2010.

OTERKUS, E.; GUVEN, I.; MADENCI, E. Impact damage assessment by using peridynamic theory. *Central European Journal of Engineering*, v. 2, n. 4, p. 523–531, 2012.

PORTER, D.; STIRLING, D. *Integral equations: a practical treatment, from spectral theory to applications*. Cambridge, UK: Cambridge University Press, 1990. v. 5.

SILLING, S. Reformulation of elasticity theory for discontinuities and long-range forces. *Journal of the Mechanics and Physics of Solids*, v. 48, n. 1, p. 175–209, 2000.

SILLING, S. Linearized theory of peridynamic states. *Journal of Elasticity*, v. 99, n. 1, p. 85–111, 2010.

SILLING, S. et al. Peridynamic states and constitutive modeling. *Journal of Elasticity*, v. 88, n. 2, p. 151–184, 2007.

SILLING, S.; LEHOUCQ, R. Convergence of peridynamics to classical elasticity theory. *Journal of Elasticity*, v. 93, n. 1, p. 13–37, 2008.

SILLING, S.; ZIMMERMANN, M.; ABEYARATNE, R. Deformation of a peridynamic bar. *Journal of Elasticity*, v. 73, n. 1-3, p. 173–190, 2003.

SOKOLNIKOFF, I. S. *Mathematical Theory of Elasticity*. 2. ed. New York: McGraw-Hill, 1956.

WANG, L.; XU, J.; WANG, J. Erratum to: Static and dynamic green's functions in peridynamics. *Journal of Elasticity*, v. 126, n. 1, p. 127–127, 2017.

WANG, L.; XU, J.; WANG, J. Static and dynamic green's functions in peridynamics. *Journal of Elasticity*, v. 126, n. 1, p. 95–125, 2017.

WARREN, T. L. et al. A nonordinary state-based peridynamic method to model solid material deformation and fracture. *International Journal of Solids and Structures*, v. 46, n. 5, p. 1186–1195, 2009.

WECKNER, O.; ABEYARATNE, R. The effect of long-range forces on the dynamics of a bar. *Journal of the Mechanics and Physics of Solids*, v. 53, n. 3, p. 705–728, 2005.

WECKNER, O.; BRUNK, G.; EPTON, M. Green's functions in non-local three-dimensional linear elasticity. *Proceedings of the Royal Society A*, v. 465, n. 2111, p. 3463–3487, 2009.

ZHOU, X.; GU, X.; WANG, Y. Numerical simulations of propagation, bifurcation and coalescence of cracks in rocks. *International Journal of Rock Mechanics and Mining Sciences*, v. 80, p. 241–254, 2015.